Assimilation of FengYun Satellite Data in CMA-GFS Using Advanced Radiative Transfer Modeling System (ARMS)

Fuzhong Weng

1. CMA Earth System Modeling and Prediction Centre
2. Nanjing University of Information Science and Technology

Acknowledgements to the Supports from Peng Zhang, Jun Yang, Hao Hu, Yang Han, Yining Shi, Lei Bi, Biqing Yi, Wei Han, Lingli He and Ziqiang Zhu and many others

Common Issues in Current Fast Radiative Transfer Models Used in NWP Models

- Radiative transfer models have large uncertainties in simulating the radiances in scattering atmospheres (e.g. aerosols, clouds and precipitation).

- Large biases are found at surface sensitive channels over land and behave differently from one model to another.

- Radiative transfer schemes solve only for radiative intensity. The instruments at UV, visible, and microwave wavelengths sensitive to polarization are not well simulated.

Advanced Radiative Transfer Modeling System (ARMS)

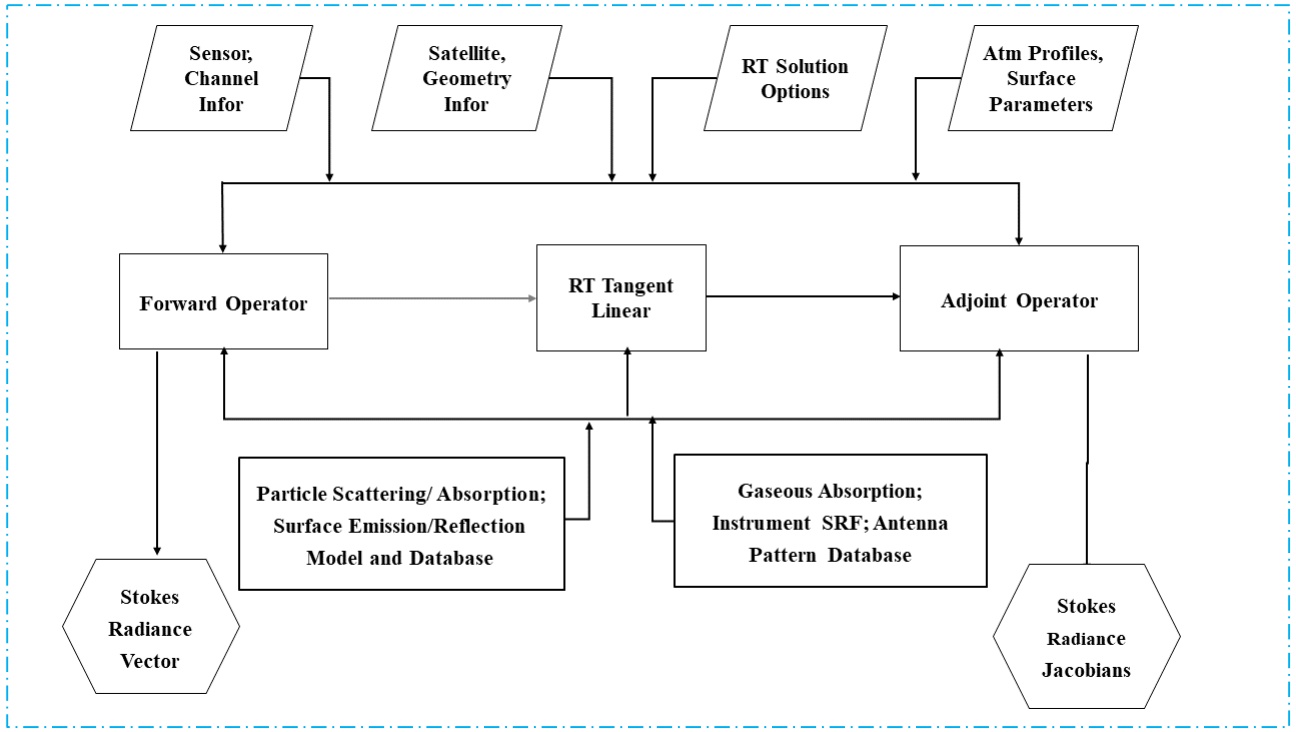

FY-3A MWTS
FY-3A MWHS
FY-3B MWTS
FY-3B MWHS
FY-3C MWTS-2
FY-3C-MWHS-2
FY-3D MWTS-2
FY-3D MWHS-2
FY-3 B/C/D/F/G MWRI
FY-3 B/C VIRR
FY-3C MERSI
FY-3C IRAS
FY-3D MERSI-2
FY-3D HIRAS
FY-4M MWS
FY-3E MWTS
FY-3E MWHS
FY-3E-HIRAS
FY-4A /B/C GIIRS
FY-4A/B/C AGRI
HY-2 MWR

NOAA 15 to 19 AMSU-A
NOAA 18-19 MHS
NOAA 18-19 HIRS
NOAA 15-19 AVHRR
SNPP/NOAA-20 ATMS
SNPP/NOAA-20 CrIS
SNPP/NOAA-20 VIIRS
METOP-A to C IASI
METOP-A to C IASI
METOP-A to C AMSU-A
METOP-A to C AVHRR
JAXA AMSR2
NASA GMI
EOS Aqua AIRS
EOS Terra/Aqua MODIS

ARMS Special Features:

RT Solvers: Emission-based, DA, P2S, **VDISORT**

Particle and Hydrometeor LUTs:

Scattering and absorption coefficients , full phase matrix elements from **T-Matrix**

Surface Models: **More physically-based models**

Atmospheric Transmittance :

more instruments from **China FY and HY satellite missions** and commercial satellite missions

ARMS Cloud and Precipitation Optics

Ice Cloud LUT

Spectrally Consistent Scattering, Absorption, and Polarization Properties of Atmospheric Ice Crystals at Wavelengths from 0.2 to 100 μm

PING YANG,* LEI BI,* BRYAN A. BAUM,+ KUO-NAN LIOU,# GEORGE W. KATTAWAR,@ MICHAEL I. MISHCHENKO,& AND BENJAMIN COLE*

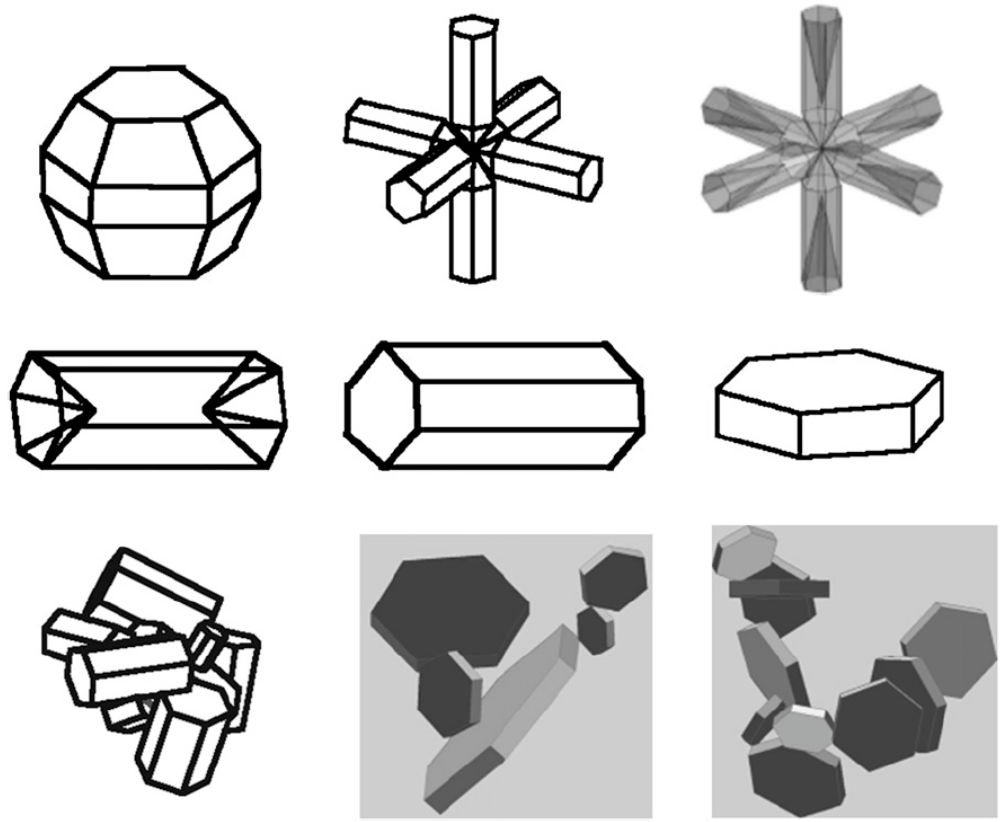

- Most Accurate Method is applied for T-Matrix

  Bi et al., 2014

  IGOM: Yang et al, 1996
- Spectral Coverage： 0.2 um - 100 um
- Particle size： 2-10000 um
- Temperature dependance
- Complete scattering information:phase matrix, scattering coefficients

ARMS Aerosol Optics

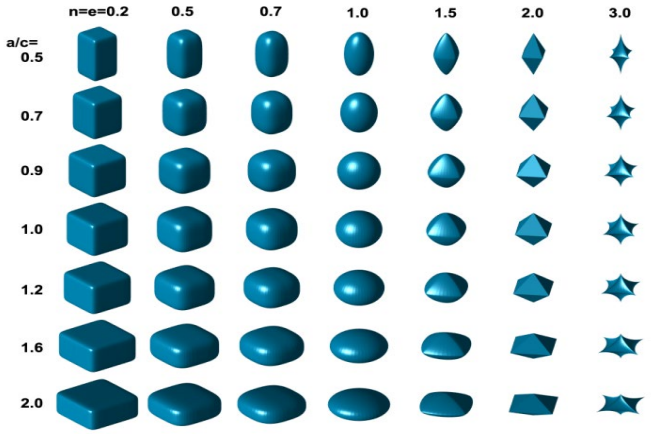

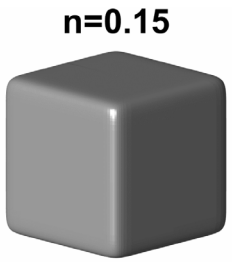

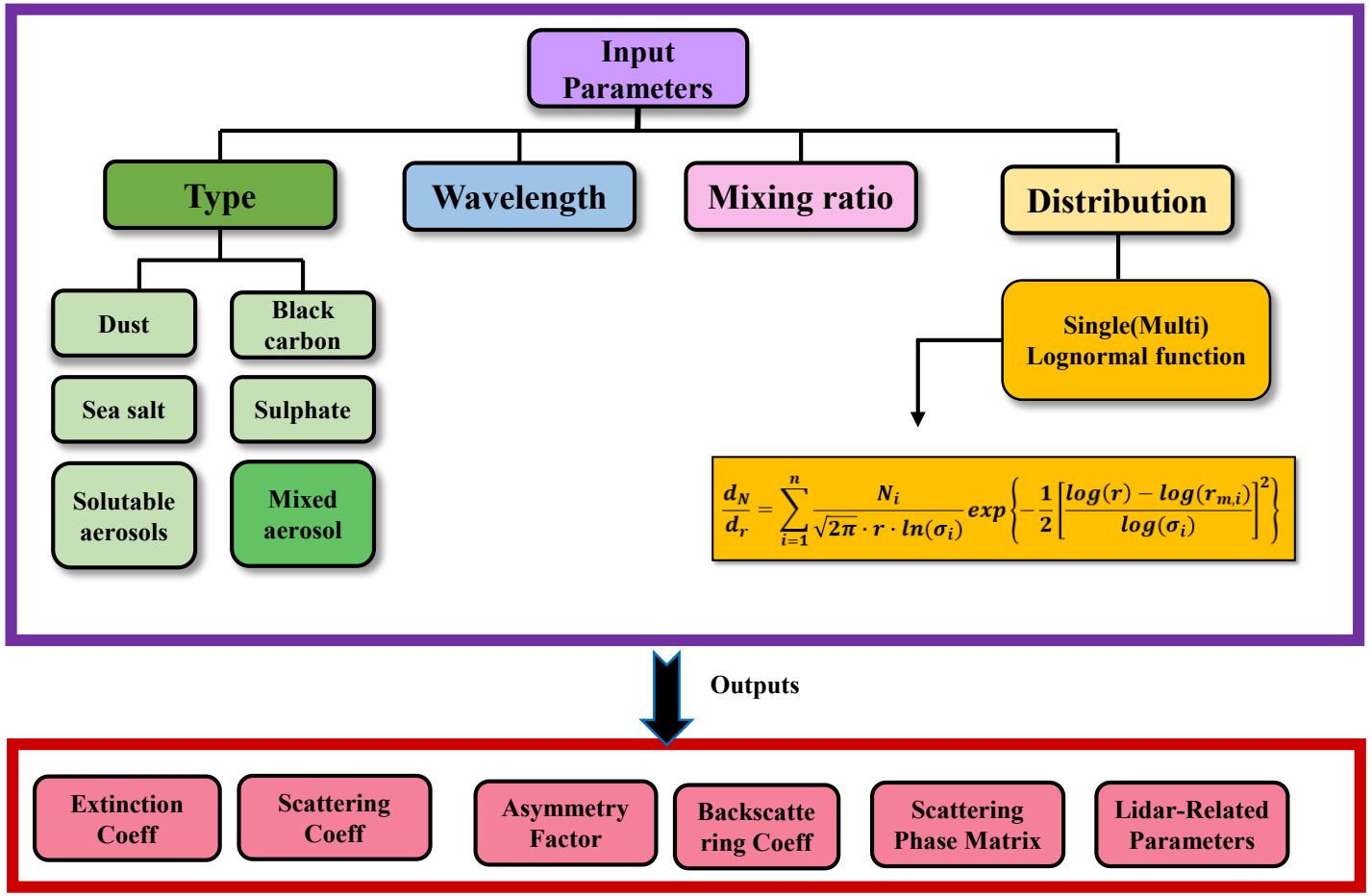

a/c, Particle short and long axis ratio

n, Surface smoothness

Bi et al., 2014, 2020

ARMS Simulations in Millimeter Wavelengths (GMI)

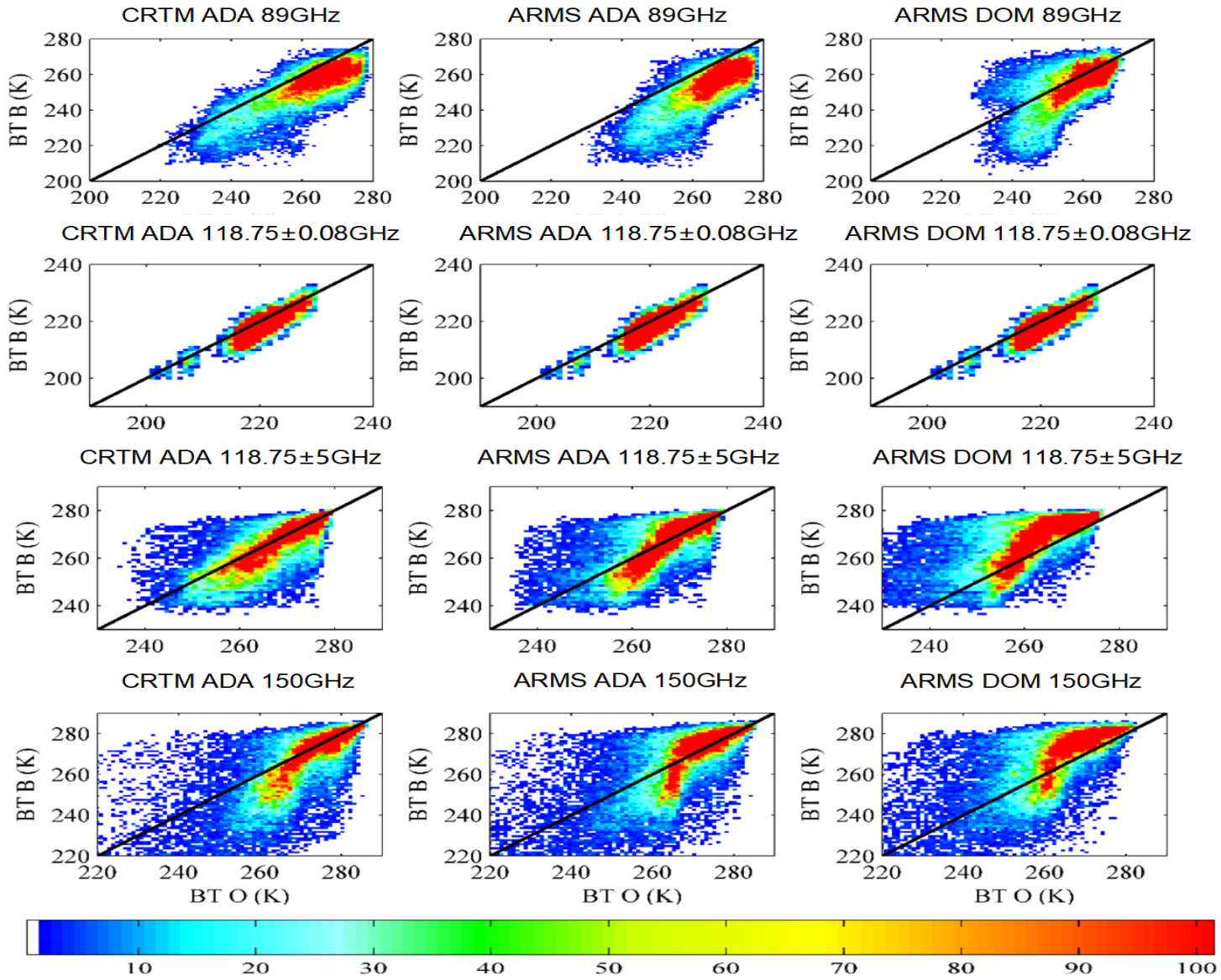

Time Period ：2018.7 - 2019.5

Profiles：ERA5

Cloud Parameters：GPM GPROF

Radiative Transfer Solvers Implemented in ARMS

$$\mu\frac{d\boldsymbol{I}(\tau,\mu,\phi)}{d\tau}=\boldsymbol{I}(\tau,\mu,\phi)-\frac{\omega(\tau)}{4\pi}\int_0^{2\pi}d\phi'\int_{-1}^{1}\boldsymbol{M}(\tau,\mu,\phi;\mu',\phi')\boldsymbol{I}(\tau,\mu',\phi')d\mu'-\boldsymbol{Q}(\tau,\mu,\phi)$$

$$\boldsymbol{Q}(\tau,\mu,\phi)=\frac{\omega(\tau)}{4\pi}\boldsymbol{M}(\tau,\mu,\phi;-\mu_0,\phi_0)\boldsymbol{S}_b\exp(-\tau/\mu_0)+(1-\omega(\tau))\boldsymbol{S}_t(\tau)$$

$$\left(I_l,I_r,I_u,I_v\right)^T \qquad \mathbf{M}=\mathbf{L}(\pi-i_2)\mathbf{S}(\Theta)\mathbf{L}(-i_1) \qquad \mathbf{S}=\begin{bmatrix}S_{11}&S_{12}&S_{13}&S_{14}\\S_{21}&S_{22}&S_{23}&S_{24}\\S_{31}&S_{32}&S_{33}&S_{34}\\S_{41}&S_{42}&S_{43}&S_{44}\end{bmatrix}$$

$$\boldsymbol{I}\left(\tau,\mu,\phi\right)=\sum_{m=0}^{2N-1}\left\{\boldsymbol{I}_m^c\left(\tau,\mu\right)cosm\left(\phi_0-\phi\right)+\boldsymbol{I}_m^s\left(\tau,\mu\right)sinm\left(\phi_0-\phi\right)\right\}$$

$$\boldsymbol{M}\left(\tau,\mu,\phi;\mu',\phi'\right)=\sum_{m=0}^{2N-1}\left\{\boldsymbol{M}_m^c\left(\tau,\mu,\mu'\right)cosm\left(\phi'-\phi\right)+\boldsymbol{M}_m^s\left(\tau,\mu,\mu'\right)sinm\left(\phi'-\phi\right)\right\}$$

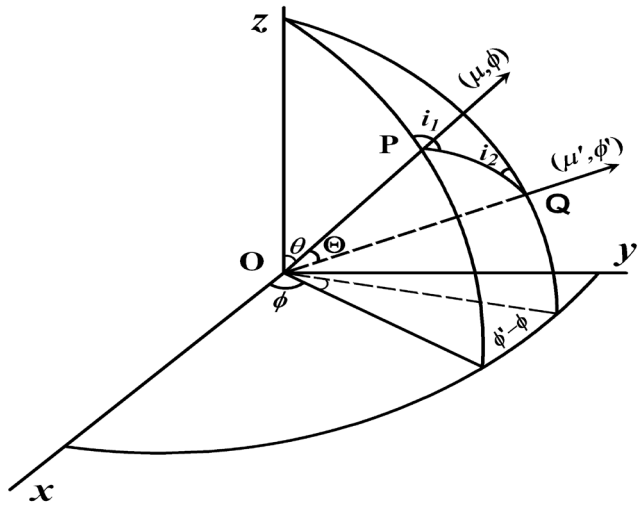

Scattering Phase Matrix is defined in POQ plane。Incoming and outgoing radiation are defined in POZ and QOZ planes

- Double and Adding (DA) - Scalar (Liu and Weng, JAS 2006)
- Polarization Two Stream Approximation (**P2S**) – First two Stokes Components (Liu and Weng, 2002, JAS)
- Vector DIscrete Ordinate Radiative Transfer (**VDISORT**) – Stokes Vector (Weng, JQSRT 1992; Schulz and Weng, 1999, JQSRT)

VDISORT V1.x

$$\mu \frac{d}{d\tau}\begin{pmatrix} \boldsymbol{I}^{c}_{m,lr}(\tau,\mu_s) \\ \boldsymbol{I}^{c}_{m,uv}(\tau,\mu_s) \\ \boldsymbol{I}^{s}_{m,lr}(\tau,\mu_s) \\ \boldsymbol{I}^{s}_{m,uv}(\tau,\mu_s) \end{pmatrix} = \begin{pmatrix} \boldsymbol{I}^{c}_{m,lr}(\tau,\mu_s) \\ \boldsymbol{I}^{c}_{m,uv}(\tau,\mu_s) \\ \boldsymbol{I}^{s}_{m,lr}(\tau,\mu_s) \\ \boldsymbol{I}^{s}_{m,uv}(\tau,\mu_s) \end{pmatrix} - \begin{pmatrix} \boldsymbol{Q}^{c}_{m,lr}(\tau,\mu_s) \\ \boldsymbol{Q}^{c}_{m,uv}(\tau,\mu_s) \\ \boldsymbol{Q}^{s}_{m,lr}(\tau,\mu_s) \\ \boldsymbol{Q}^{s}_{m,uv}(\tau,\mu_s) \end{pmatrix} -$$

$$\sum_{j=-(N+1),\,j\neq 0}^{N+1} \left\{ \begin{pmatrix} c_1\boldsymbol{M}^{c}_{m,11}(\tau,\mu_s,\mu_j) & c_1\boldsymbol{M}^{c}_{m,12}(\tau,\mu_s,\mu_j) & -c_2\boldsymbol{M}^{s}_{m,11}(\tau,\mu_s,\mu_j) & -c_2\boldsymbol{M}^{s}_{m,12}(\tau,\mu_s,\mu_j) \\ c_1\boldsymbol{M}^{c}_{m,21}(\tau,\mu_s,\mu_j) & c_1\boldsymbol{M}^{c}_{m,22}(\tau,\mu_s,\mu_j) & -c_2\boldsymbol{M}^{s}_{m,21}(\tau,\mu_s,\mu_j) & -c_2\boldsymbol{M}^{s}_{m,22}(\tau,\mu_s,\mu_j) \\ c_2\boldsymbol{M}^{s}_{m,11}(\tau,\mu_s,\mu_j) & c_2\boldsymbol{M}^{s}_{m,12}(\tau,\mu_s,\mu_j) & c_2\boldsymbol{M}^{c}_{m,11}(\tau,\mu_s,\mu_j) & c_2\boldsymbol{M}^{c}_{m,12}(\tau,\mu_s,\mu_j) \\ c_2\boldsymbol{M}^{s}_{m,21}(\tau,\mu_s,\mu_j) & c_2\boldsymbol{M}^{s}_{m,22}(\tau,\mu_s,\mu_j) & c_2\boldsymbol{M}^{c}_{m,21}(\tau,\mu_s,\mu_j) & c_2\boldsymbol{M}^{c}_{m,22}(\tau,\mu_s,\mu_j) \end{pmatrix} \begin{pmatrix} \boldsymbol{I}^{c}_{m,lr}(\tau,\mu_j) \\ \boldsymbol{I}^{c}_{m,uv}(\tau,\mu_j) \\ \boldsymbol{I}^{s}_{m,lr}(\tau,\mu_j) \\ \boldsymbol{I}^{s}_{m,uv}(\tau,\mu_j) \end{pmatrix} \right\}$$

$$c_1 = \frac{\omega(\tau)}{4} w_j\left(1+\delta_{0m}\right); \quad c_2 = \frac{\omega(\tau)}{4} w_j\left(1-\delta_{0m}\right); \quad s = -(N+1),\cdots,(N+1) \ \textit{and} \ s \neq 0$$

$$\boldsymbol{i}_m(\tau,\mu_s) = \begin{pmatrix} \boldsymbol{I}^{c}_{m,lr}(\tau,\mu_s) \\ \boldsymbol{I}^{c}_{m,uv}(\tau,\mu_s) \\ \boldsymbol{I}^{s}_{m,lr}(\tau,\mu_s) \\ \boldsymbol{I}^{s}_{m,uv}(\tau,\mu_s) \end{pmatrix}; \quad \boldsymbol{q}_m(\tau,\mu_s) = -\begin{pmatrix} \boldsymbol{Q}^{c}_{m,lr}(\tau,\mu_s) \\ \boldsymbol{Q}^{c}_{m,uv}(\tau,\mu_s) \\ \boldsymbol{Q}^{s}_{m,lr}(\tau,\mu_s) \\ \boldsymbol{Q}^{s}_{m,uv}(\tau,\mu_s) \end{pmatrix}$$

Weng, F., 1992: A multi-layer discrete-ordinate method for vector radiative transfer in vertically-inhomogeneous; emitting and scattering atmosphere, Part I: Theory, *J. Quant. Spectrosc. Radiat. Trans.*, **47**, 19-33

Most solvers including VDISORT only deal with a composite Fourier vector which consists of cosine Fourier harmonics of first two Stokes components and sine Fourier harmonics of the 3rd and 4th Stokes components; thus solvers are valid for spherical or randomly oriented particles, unpolarized source, specular surface reflection .

VDISORT V2.x

$$\mu\frac{d}{d\tau}\begin{pmatrix} \boldsymbol{I}^{c}_{m,lr}(\tau,\mu_s) \\ \boldsymbol{I}^{c}_{m,uv}(\tau,\mu_s) \\ \boldsymbol{I}^{s}_{m,lr}(\tau,\mu_s) \\ \boldsymbol{I}^{s}_{m,uv}(\tau,\mu_s) \end{pmatrix} = \begin{pmatrix} \boldsymbol{I}^{c}_{m,lr}(\tau,\mu_s) \\ \boldsymbol{I}^{c}_{m,uv}(\tau,\mu_s) \\ \boldsymbol{I}^{s}_{m,lr}(\tau,\mu_s) \\ \boldsymbol{I}^{s}_{m,uv}(\tau,\mu_s) \end{pmatrix} - \begin{pmatrix} \boldsymbol{Q}^{c}_{m,lr}(\tau,\mu_s) \\ \boldsymbol{Q}^{c}_{m,uv}(\tau,\mu_s) \\ \boldsymbol{Q}^{s}_{m,lr}(\tau,\mu_s) \\ \boldsymbol{Q}^{s}_{m,uv}(\tau,\mu_s) \end{pmatrix} -$$

$$\sum_{j=-(N+1),\,j\neq 0}^{N+1}\left\{\begin{pmatrix} c_1\boldsymbol{M}^{c}_{m,11}(\tau,\mu_s,\mu_j) & c_1\boldsymbol{M}^{c}_{m,12}(\tau,\mu_s,\mu_j) & -c_2\boldsymbol{M}^{s}_{m,11}(\tau,\mu_s,\mu_j) & -c_2\boldsymbol{M}^{s}_{m,12}(\tau,\mu_s,\mu_j) \\ c_1\boldsymbol{M}^{c}_{m,21}(\tau,\mu_s,\mu_j) & c_1\boldsymbol{M}^{c}_{m,22}(\tau,\mu_s,\mu_j) & -c_2\boldsymbol{M}^{s}_{m,21}(\tau,\mu_s,\mu_j) & -c_2\boldsymbol{M}^{s}_{m,22}(\tau,\mu_s,\mu_j) \\ c_2\boldsymbol{M}^{s}_{m,11}(\tau,\mu_s,\mu_j) & c_2\boldsymbol{M}^{s}_{m,12}(\tau,\mu_s,\mu_j) & c_2\boldsymbol{M}^{c}_{m,11}(\tau,\mu_s,\mu_j) & c_2\boldsymbol{M}^{c}_{m,12}(\tau,\mu_s,\mu_j) \\ c_2\boldsymbol{M}^{s}_{m,21}(\tau,\mu_s,\mu_j) & c_2\boldsymbol{M}^{s}_{m,22}(\tau,\mu_s,\mu_j) & c_2\boldsymbol{M}^{c}_{m,21}(\tau,\mu_s,\mu_j) & c_2\boldsymbol{M}^{c}_{m,22}(\tau,\mu_s,\mu_j) \end{pmatrix}\begin{pmatrix} \boldsymbol{I}^{c}_{m,lr}(\tau,\mu_j) \\ \boldsymbol{I}^{c}_{m,uv}(\tau,\mu_j) \\ \boldsymbol{I}^{s}_{m,lr}(\tau,\mu_j) \\ \boldsymbol{I}^{s}_{m,uv}(\tau,\mu_j) \end{pmatrix}\right\}$$

$$c_1 = \frac{\omega(\tau)}{4}w_j\left(1+\delta_{0m}\right);\quad c_2 = \frac{\omega(\tau)}{4}w_j\left(1-\delta_{0m}\right);\quad s = -(N+1),\cdots,(N+1)\ \ and\ \ s\neq 0$$

$$\boldsymbol{i}_m(\tau,\mu_s) = \begin{pmatrix} \boldsymbol{I}^{c}_{m,lr}(\tau,\mu_s) \\ \boldsymbol{I}^{c}_{m,uv}(\tau,\mu_s) \\ \boldsymbol{I}^{s}_{m,lr}(\tau,\mu_s) \\ \boldsymbol{I}^{s}_{m,uv}(\tau,\mu_s) \end{pmatrix};\quad \boldsymbol{q}_m(\tau,\mu_s) = -\begin{pmatrix} \boldsymbol{Q}^{c}_{m,lr}(\tau,\mu_s) \\ \boldsymbol{Q}^{c}_{m,uv}(\tau,\mu_s) \\ \boldsymbol{Q}^{s}_{m,lr}(\tau,\mu_s) \\ \boldsymbol{Q}^{s}_{m,uv}(\tau,\mu_s) \end{pmatrix}$$

Zhu, Z. and F. Weng, 2023； Vector radiative transfer in a vertically inhomogeneous scattering and emitting atmosphere: Part 1 discrete ordinate theory; *Submitted to J. Atmos. Sci*

The VDISORT2.x solves the composite Fourier vector which consists of Stokes harmonic components and it is applicable for spherical or any oriented particles, polarized source, many types of surface reflection.

Comparison of VDISORT 2.0 Simulations with Benchmark

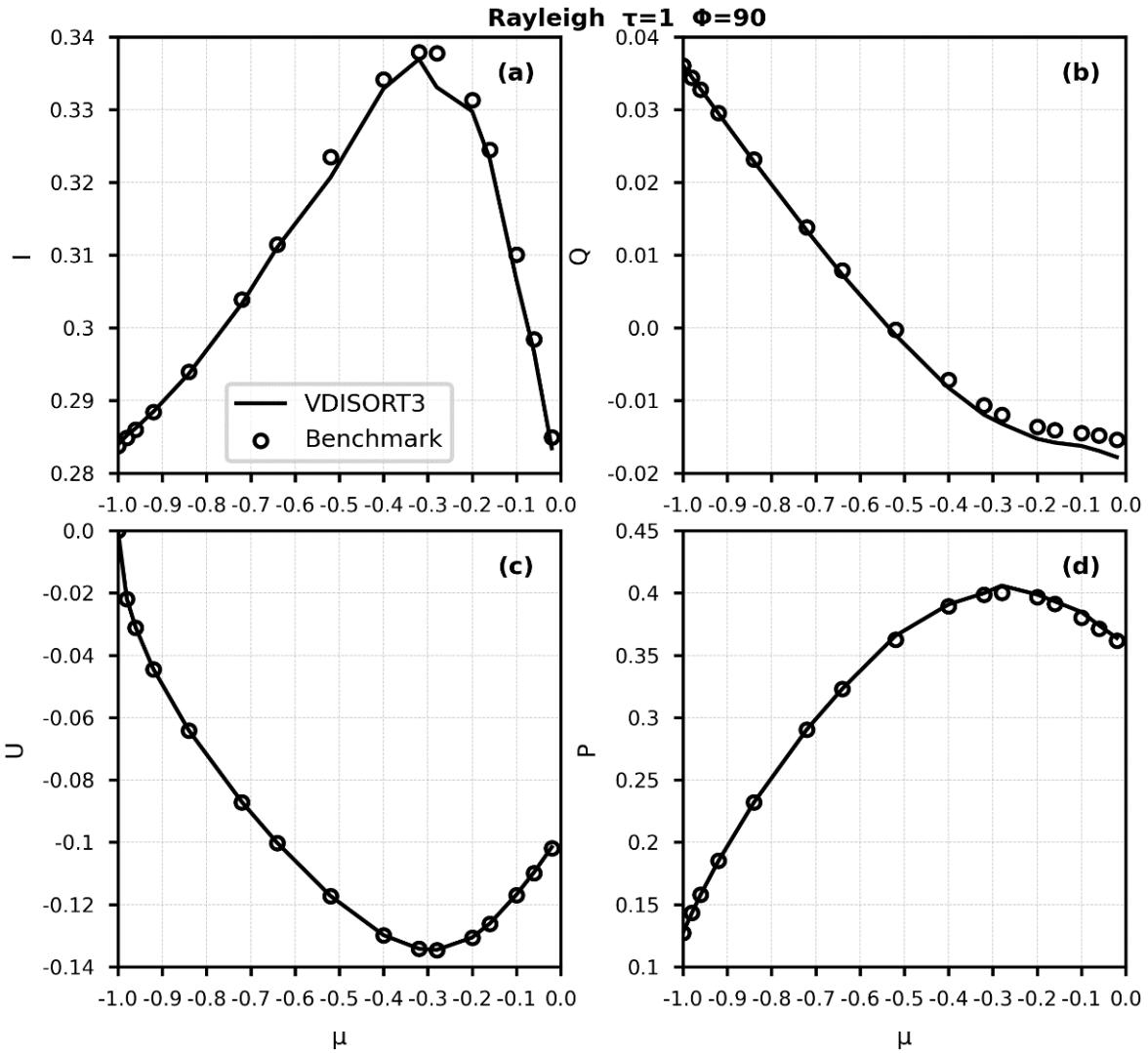

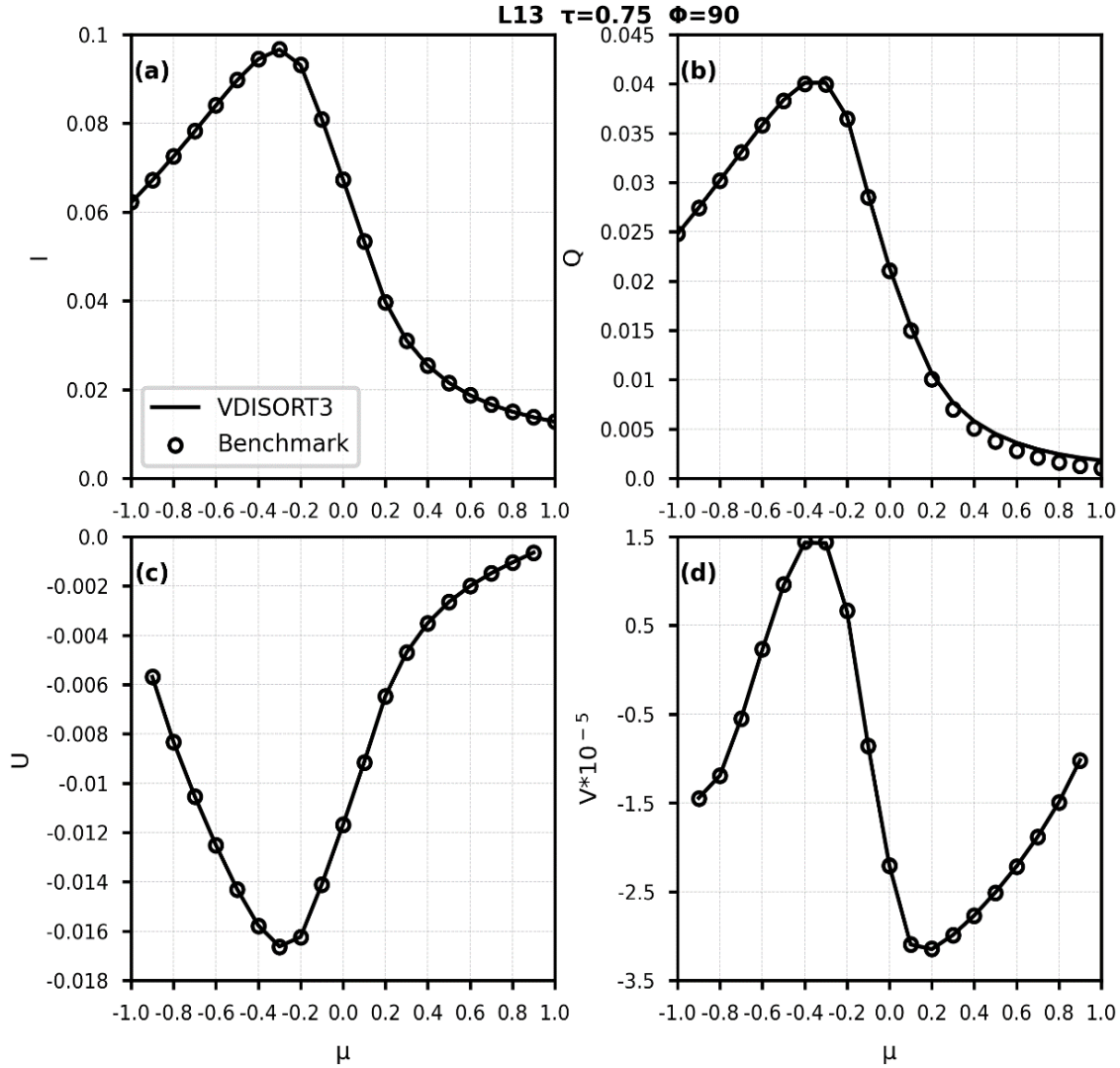

VDISORT 2.0 Simulations with Polarized Source

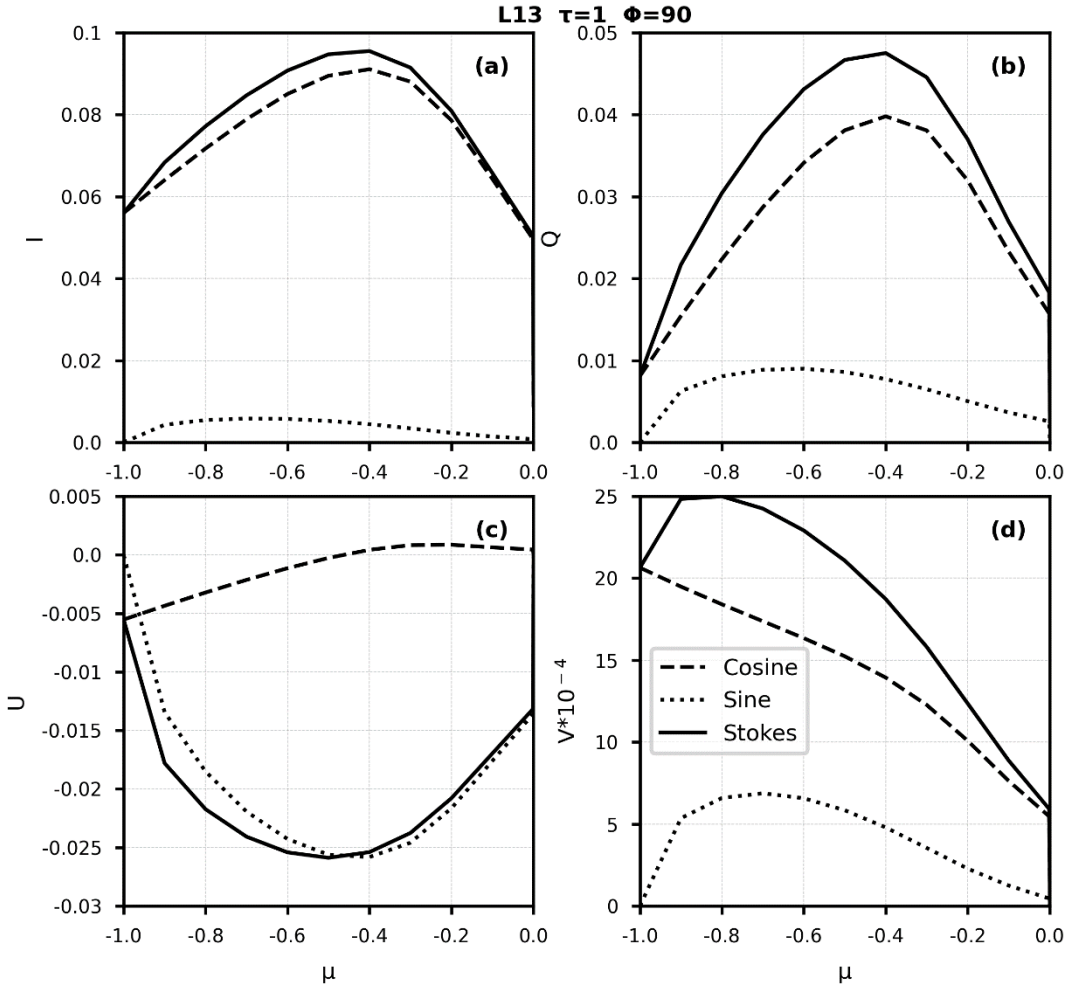

Inputs:

Polarized sources: $\boldsymbol{S}_b = \left(0.7\pi, 0.3\pi, 0.2\pi, 0.05\pi\right)^T$

Spherical Scattering: L13 scattering matrix

The contribution from the composite Fourier sine component is significant when the polarized source is present in radiative transfer equation.

Lower Boundary Condition for Current Fast RT Models

$$\mathbf{I}(\mu,\phi)=\mathbf{E}\mathbf{S}_t+\frac{1}{\pi}\int_0^{2\pi}\int_0^{1}\mathbf{A}(\mu,\phi;-\mu',\phi')\mathbf{I}(-\mu',\phi')d\mu'd\phi'+\mathbf{A}(\mu,\phi;-\mu_0',\phi_0')\frac{\mu_0\mathbf{S}_b}{\pi}\exp(-\tau_L/\mu_0)$$

$$\mathbf{I}=[I_l,I_r,U,V]$$

$$\mathbf{A}=\begin{pmatrix} A_{vvvv} & A_{vhvh} & 0 & 0 \\ A_{hvhv} & A_{hhhh} & 0 & 0 \\ 0 & 0 & \mathrm{Re}(A_{vvhh}+A_{vhhv}) & \mathrm{Im}(A_{hhvv}+A_{hvvh}) \\ 0 & 0 & \mathrm{Im}(A_{vvhh}+A_{vhhv}) & \mathrm{Re}(A_{hhvv}-A_{hvvh}) \end{pmatrix}$$

$$\mathbf{E}(\theta_s,\varphi_s)=\mathbf{I}_i-\int_0^{\pi/2}\sin\theta_i d\theta_i\int_0^{2\pi}d\varphi_i\mathbf{A}\mathbf{I}_i \qquad \mathbf{I}_i=\begin{pmatrix}1\\1\\0\\0\end{pmatrix}$$

$$\mathbf{A}=\mathbf{A}^c+\left\langle\mathbf{A}^i_{SPM}\right\rangle$$

$$\mathbf{A}^c(\theta_i,\varphi_i;\theta_s,\varphi_s)=\frac{P(S_x,S_y)S(\theta_i,\theta_s)}{4\cos\theta_i\cos\theta_s\cos^4\beta}\times\mathbf{L}(\pi-i_2)\mathbf{R}^c(\theta_{il},\varphi_{il};\theta_{sl},\varphi_{sl})\mathbf{L}(-i_1)$$

$$P(S_x,S_y)=\frac{F(S_x,S_y)}{2\pi\sigma_u\sigma_c}\exp\left(-\frac{S_x^2}{2\sigma_u^2}-\frac{S_y^2}{2\sigma_c^2}\right)$$

$$\left\langle\mathbf{A}^i_{SPM}(\theta_i,\varphi_i;\theta_s,\varphi_s)\right\rangle=\int_{-\infty}^{\infty}dS_y'\int_{-\infty}^{\infty}dS_x'P(S_x,S_y)\times S(\theta_i,\theta_s)\mathbf{A}^i_{SPM}(\theta_i,\varphi_i;\theta_s,\varphi_s)$$

$$\mathbf{A}^i_{SPM}(\theta_i,\varphi_i;\theta_s,\varphi_s)=\mathbf{L}(\alpha_2)\mathbf{R}^i(\theta_{il},\varphi_{il};\theta_{sl},\varphi_{sl})\cdot\mathbf{L}(\alpha_1)k_0^4\cos\theta_{il}hW_s(k_x,k_y)$$

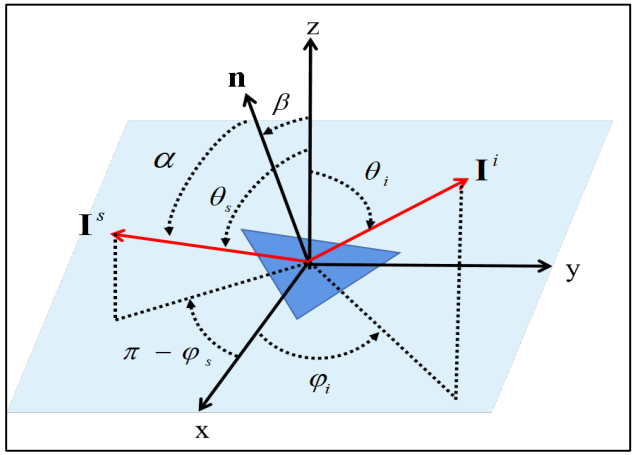

Liu, Q. , F. Weng and S. English, 2011: 2011: An Improved Fast Microwave Water Emissivity model: *IEEE Trans. Geosci. Remote Sens.,* 1238-1250, DOI: 10.1109/TGRS.2010.2064779.

Lower Boundary Condition for VDISORT2.x

$$\mathbf{I}(\mu,\phi)=\mathbf{E}\mathbf{S}_t+\frac{1}{\pi}\int_0^{2\pi}\int_0^{1}\mathbf{A}(\mu,\phi;-\mu',\phi')\mathbf{I}(-\mu',\phi')d\mu'd\phi'+\mathbf{A}(\mu,\phi;-\mu_0',\phi_0')\frac{\mu_0\mathbf{S}_b}{\pi}\exp(-\tau_L/\mu_0)$$

$$\mathbf{I}=[I_l,I_r,U,V]$$

$$\mathbf{A}=\begin{pmatrix} A_{vvvv} & A_{vhvh} & \mathrm{Re}(A_{vhvv}) & \mathrm{Im}(A_{vhvv}) \\ A_{hvhv} & A_{hhhh} & \mathrm{Re}(A_{hhhv}) & \mathrm{Im}(A_{hhhv}) \\ 2\,\mathrm{Re}(A_{vvhv}) & 2\,\mathrm{Re}(A_{vhhh}) & \mathrm{Re}(A_{vvhh}+A_{vhhv}) & \mathrm{Im}(A_{hhvv}+A_{hvvh}) \\ 2\,\mathrm{Im}(A_{vvhv}) & 2\,\mathrm{Im}(A_{vhhh}) & \mathrm{Im}(A_{vvhh}+A_{vhhv}) & \mathrm{Re}(A_{hhvv}-A_{hvvh}) \end{pmatrix}$$

$$\mathbf{E}(\theta_s,\varphi_s)=\mathbf{I}_i-\int_0^{\pi/2}\sin\theta_i d\theta_i\int_0^{2\pi}d\varphi_i\mathbf{A}\mathbf{I}_i \qquad \mathbf{I}_i=\begin{pmatrix}1\\1\\0\\0\end{pmatrix}$$

$$\mathbf{A}=\mathbf{A}^c+\left\langle\mathbf{A}^i_{SPM}\right\rangle$$

$$\mathbf{A}^c(\theta_i,\varphi_i;\theta_s,\varphi_s)=\frac{P(S_x,S_y)S(\theta_i,\theta_s)}{4\cos\theta_i\cos\theta_s\cos^4\beta}\times\mathbf{L}(\pi-i_2)\mathbf{R}^c(\theta_{il},\varphi_{il};\theta_{sl},\varphi_{sl})\mathbf{L}(-i_1)$$

$$P(S_x,S_y)=\frac{F(S_x,S_y)}{2\pi\sigma_u\sigma_c}\exp\left(-\frac{S_x^2}{2\sigma_u^2}-\frac{S_y^2}{2\sigma_c^2}\right)$$

$$\left\langle\mathbf{A}^i_{SPM}(\theta_i,\varphi_i;\theta_s,\varphi_s)\right\rangle=\int_{-\infty}^{\infty}dS_y'\int_{-\infty}^{\infty}dS_x'P(S_x,S_y)\times S(\theta_i,\theta_s)\mathbf{A}^i_{SPM}(\theta_i,\varphi_i;\theta_s,\varphi_s)$$

$$\mathbf{A}^i_{SPM}(\theta_i,\varphi_i;\theta_s,\varphi_s)=\mathbf{L}(\alpha_2)\mathbf{R}^i(\theta_{il},\varphi_{il};\theta_{sl},\varphi_{sl})\cdot\mathbf{L}(\alpha_1)k_0^4\cos\theta_{il}hW_s(k_x,k_y)$$

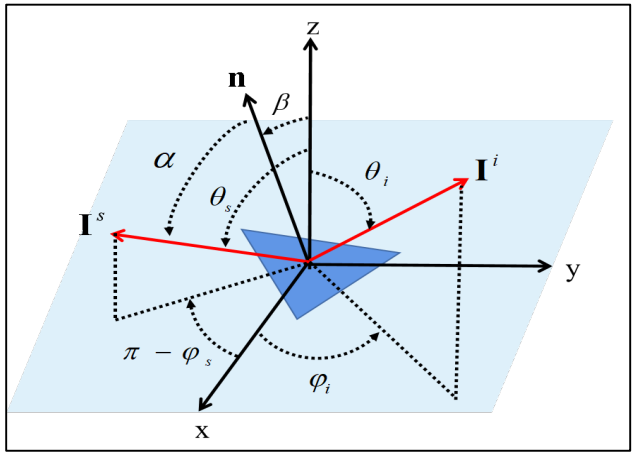

He, L. and F. Weng, 2022: Ocean Microwave Bidirectional Reflectivity Model Developed from Two-scale Roughness Theory *; Submitted to Advances in Atmospheric Science*

Polarized BRDF (pBRDF) Model for Oceans

Two-Scale Model (TSM)

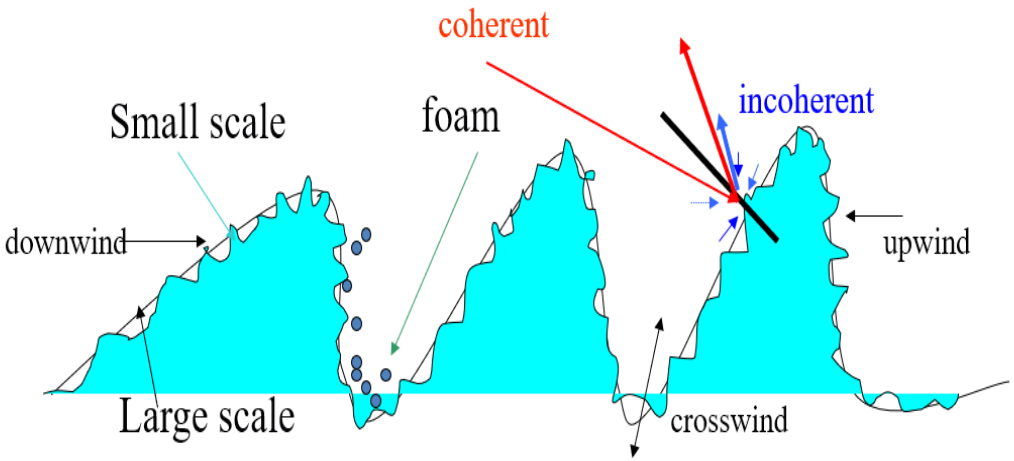

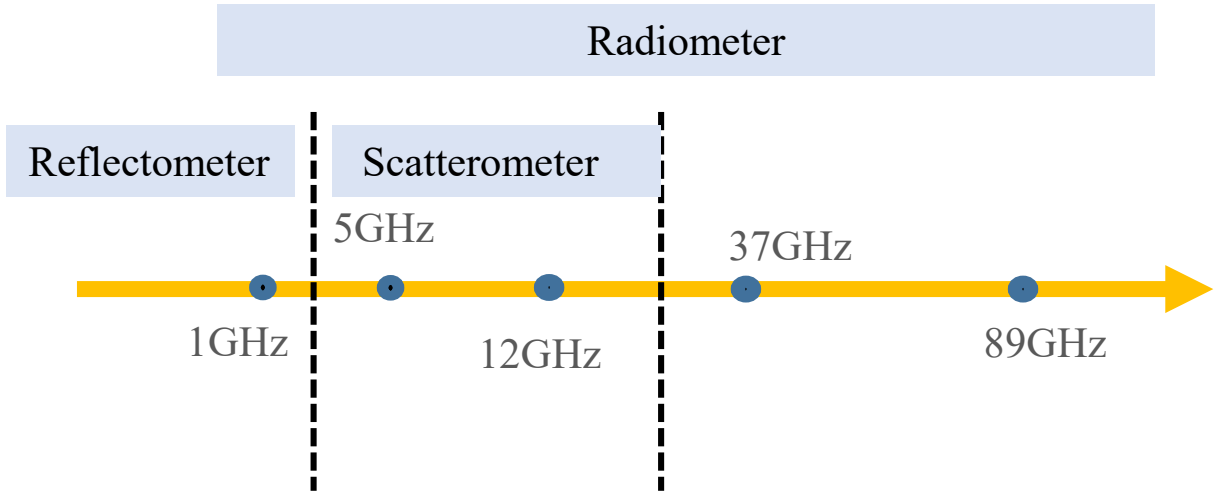

- Large scale roughness is generated gravity wave and small scale roughness is related capillary waves
- Coherent and non-coherent reflection and scattering from both scales
- Coherent term is derived from geometric optics
- Non-coherent is derived from small perturbation model (SPM)
- TSM is valid for small to medium incidence angles and moderate wind speed

For details, please see poster presentation 10p.04 by He and Weng

Windspeed Dependance of pBRDF (A) Matrix

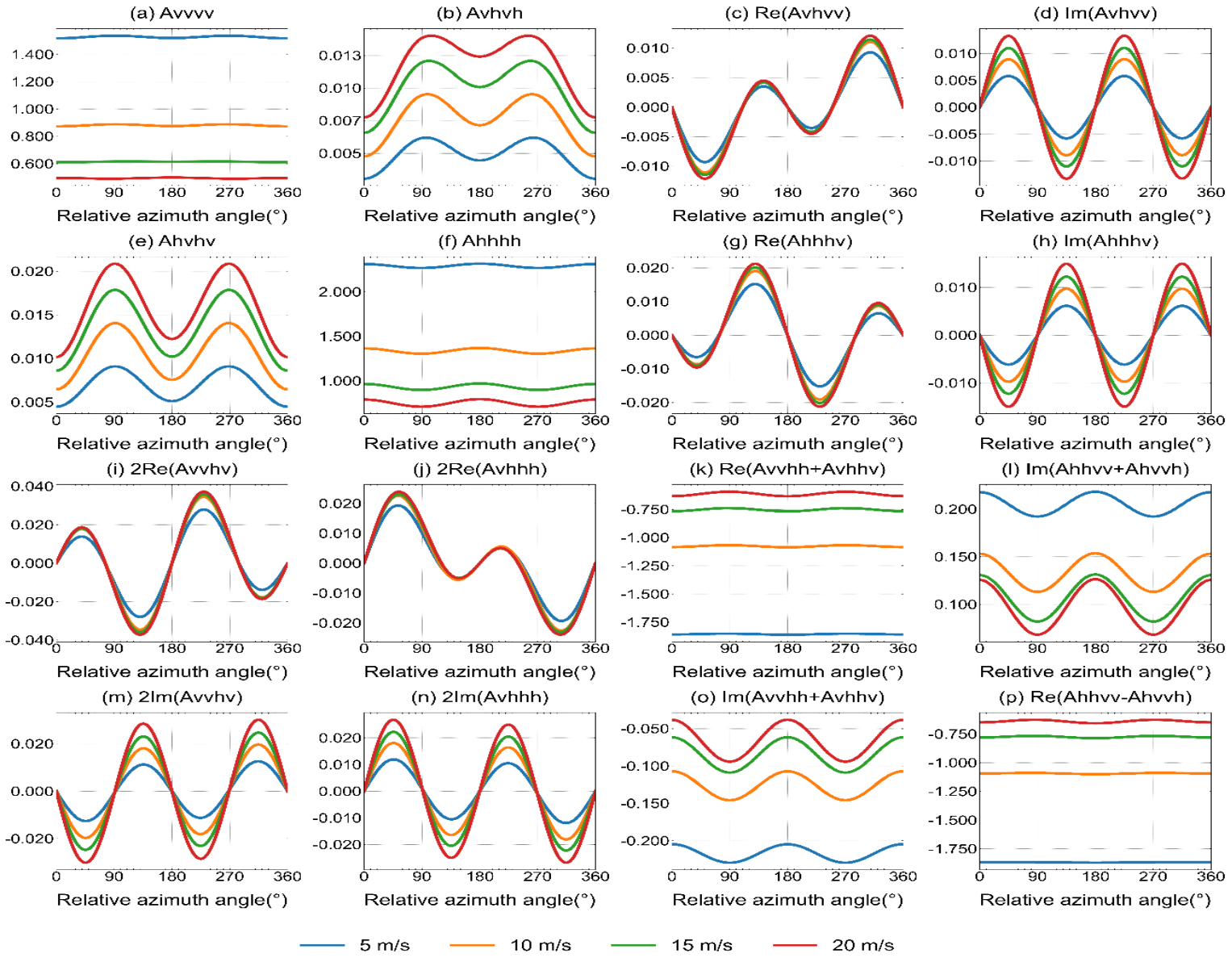

For a specific geometry

$$\theta_i = \theta_s, \varphi_i = \varphi_s$$

Frequency = 37GHz
Zenith angle = 45°
SST = 285K
SSS = 35‰

1. **pBDRF elements can have a unit of inverse solid angle (sr^{-1})**
2. **Thus, the magnitudes can be greater than 1**
3. **As wind speed increases, the harmonic amplitudes of some elements increases significantly**

Major Applications of pBDRF

Passive Sensor: Microwave Imager

$$\mathbf{E}(\theta_s,\varphi_s)=\mathbf{I}_i-\int_0^{2\pi}\int_0^{\pi/2}\mathbf{A}\cdot\mathbf{I}_i\cos\theta_i\sin\theta_i d\theta_i d\varphi_i$$

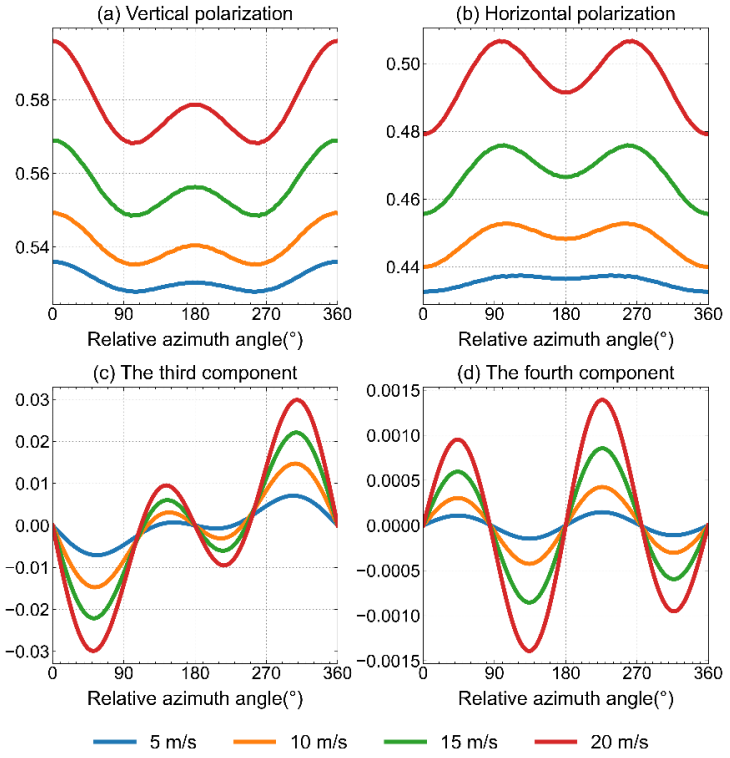

Active Sensor: Scatterometer

$$\theta_i=\theta_s,\varphi_i=\varphi_s+\pi$$

$$\sigma_{vv}=4\pi A_{vvvv}\cos\theta_i\cos\theta_s$$

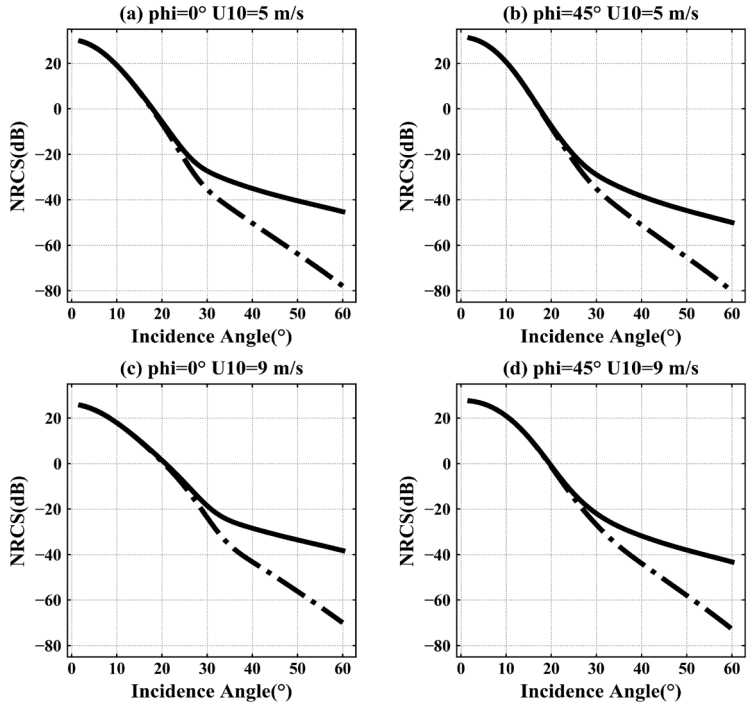

Active Sensor: Reflectormeter

$$\theta_i=\theta_s,\varphi_i=\varphi_s$$

$$\sigma_{vv}=4\pi A_{vvvv}\cos\theta_i\cos\theta_s$$

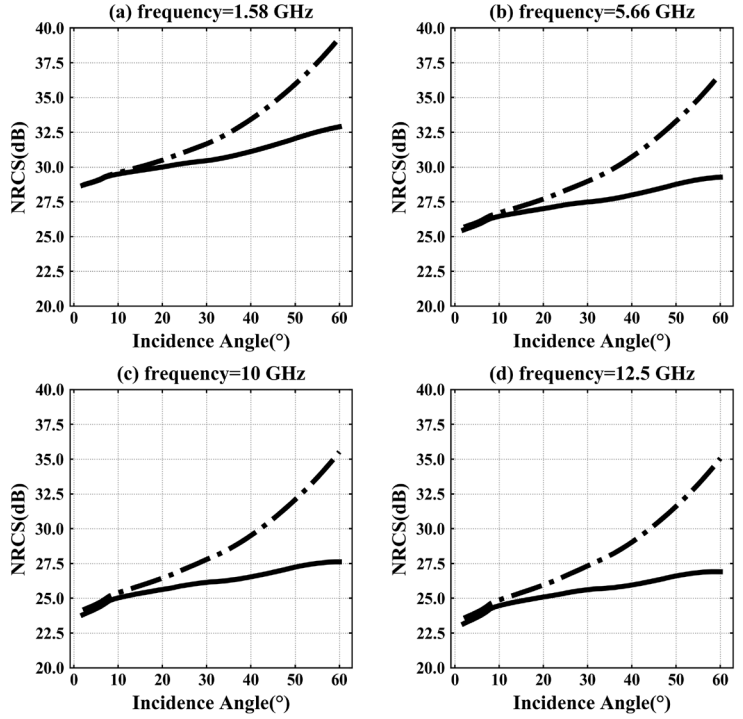

SST= 285K, SSS= 35‰, frequency=37GHz, θ_s =30°

X band

Wind Speed 10m/s

Intercomparison of pBRDF with PARMIO/FASTEM

37 GHz, 285K, observation zenith angle 30° , salinity 35‰

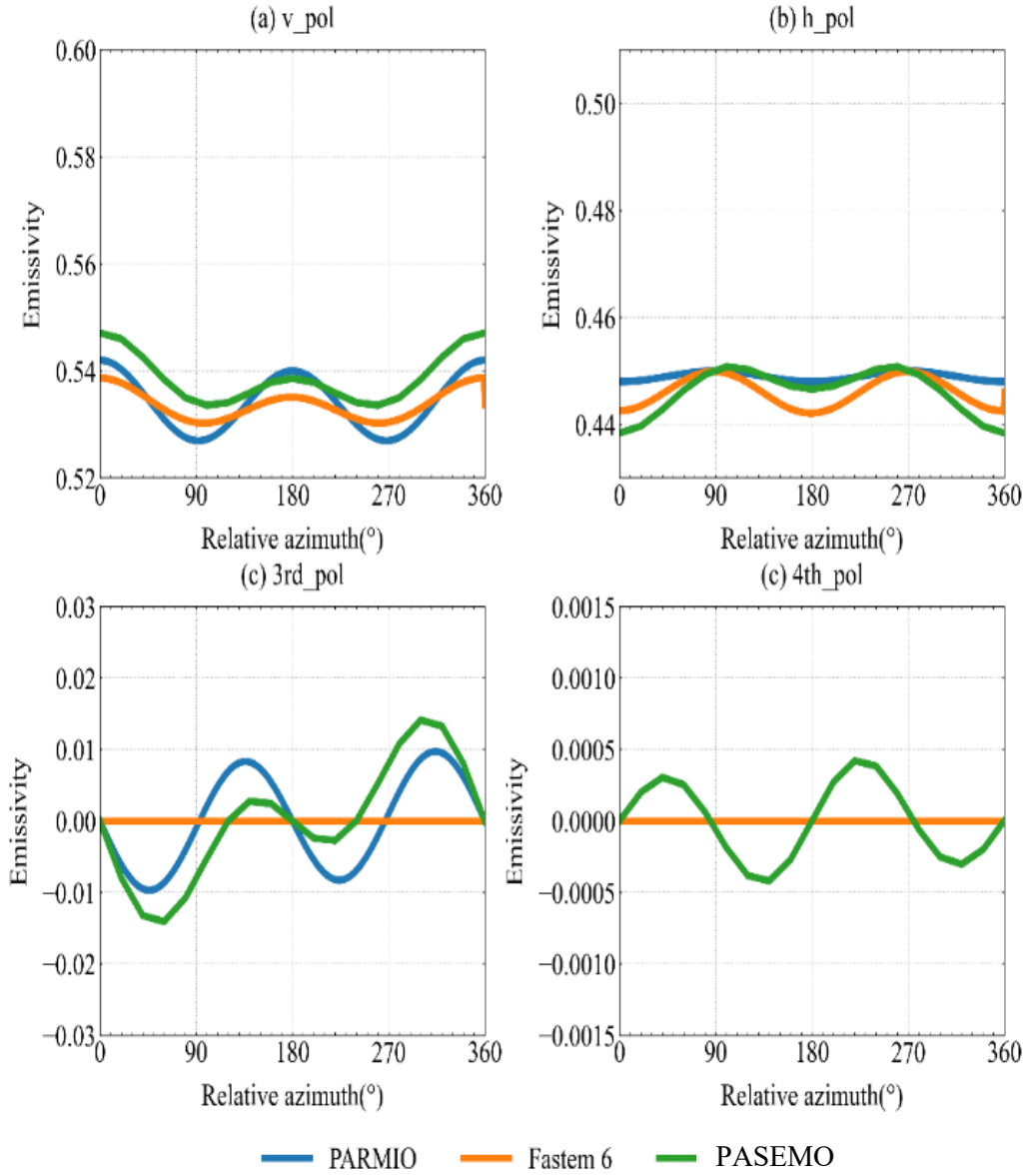

- PARMIO can not predict the fourth Stokes component at 5 m/s and 10 m/s windspeed.
- PARMIO have the opposite phases to TSEM and FASTEM in horizontal polarization at 15 and 20 m/s.
- The differences between PASEMO Stokes Emissivity Vector (SEV) and FASTEM are small in both vertical and horizontal polarization.

Normalized Radar Cross Section (NRCS) at C-Band from pBRDF and PARMIO

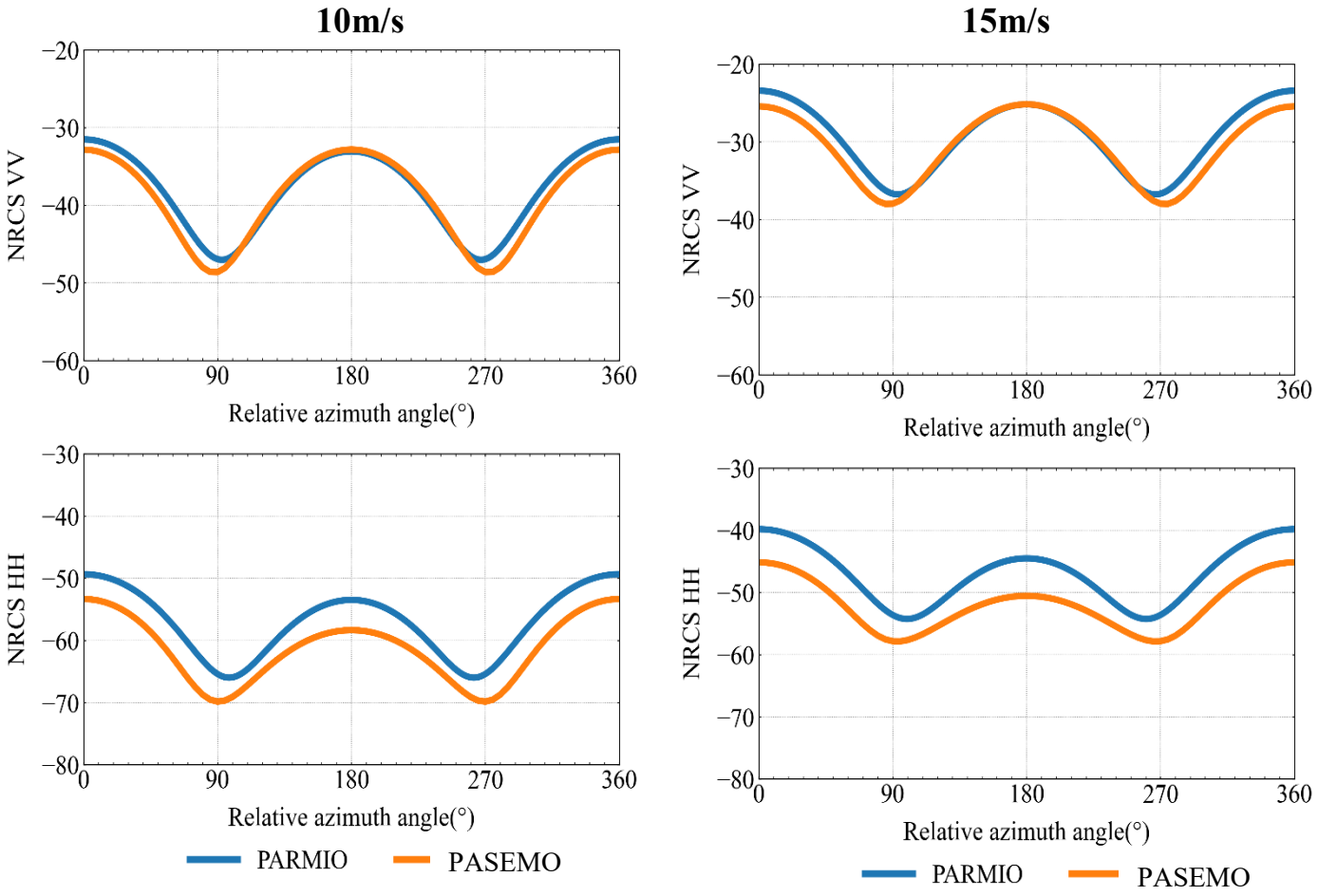

- In VV NRCS, the smallest difference appears in the downwind direction.
- VV NRCS is more consistent than HH NRCS.
- The azimuth variations of the two model are similar.

SST=285K, zenith angle = 50^0, SSS = 35‰, C band

Normalized Radar Cross Section (NRCS) from METOP-C ASCAT

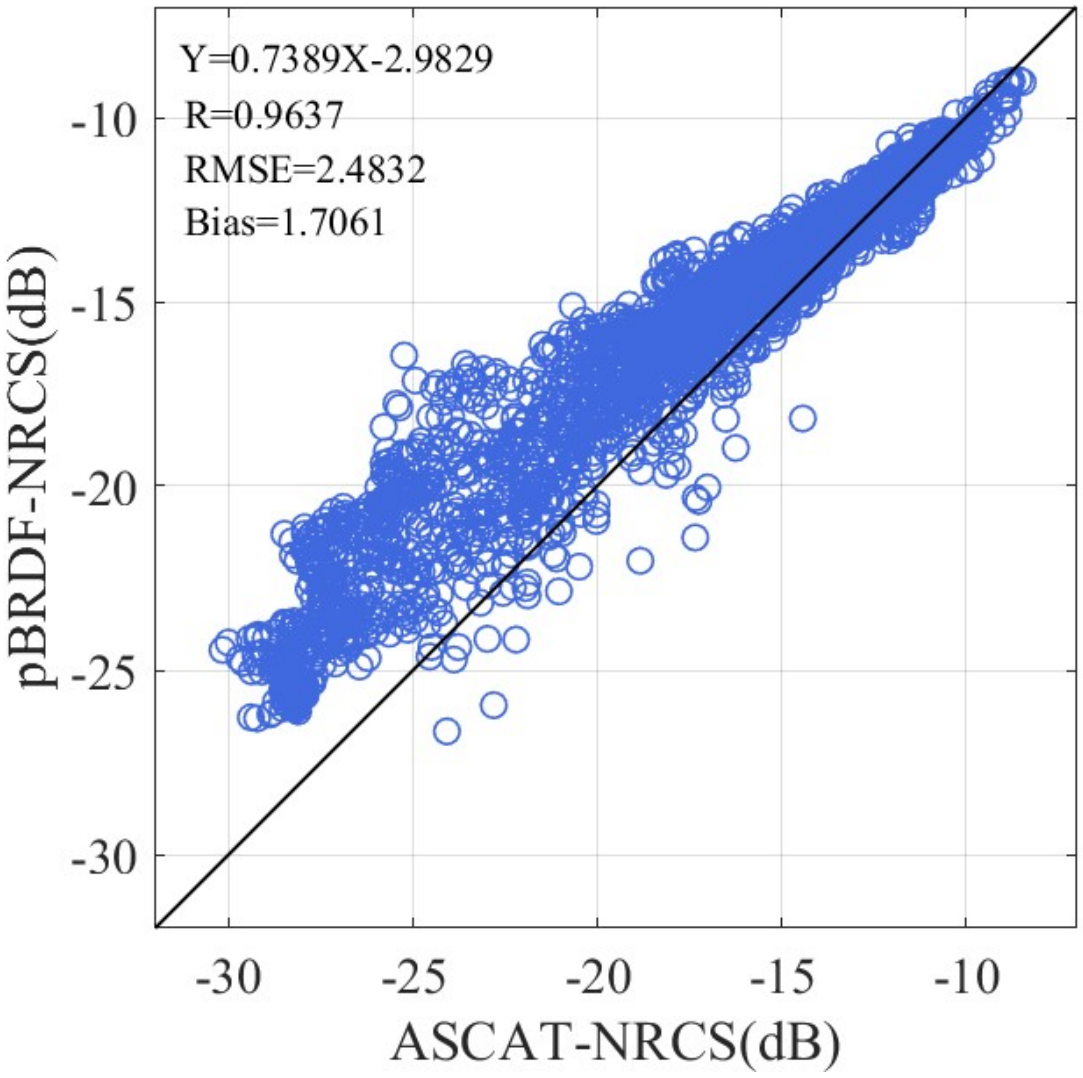

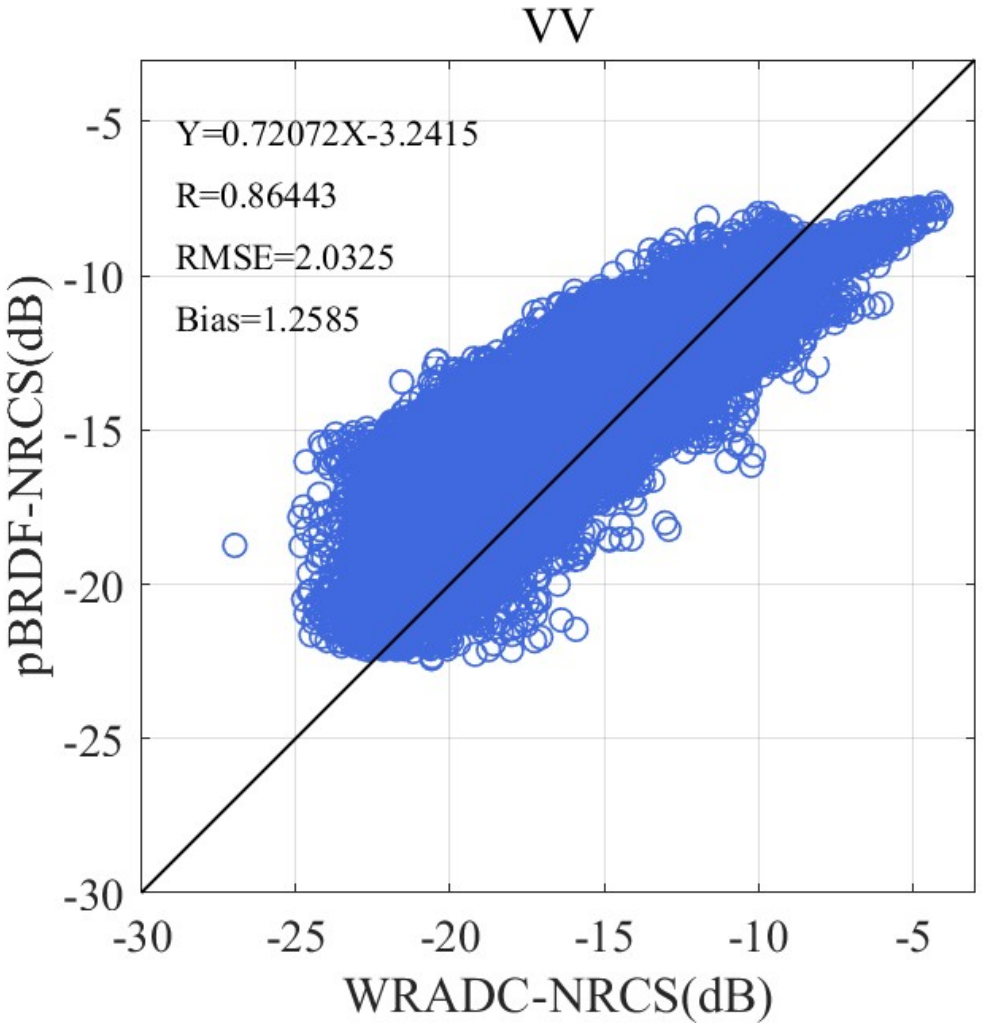

FY-3E WindRAD

Uses of ARMS in CMA Global Forecast System (GFS)

- **CMA-Global Forecast System (GFS)**
  - Vertical layer:87
  - Model top: 0.1 hPa, 63 km
  - Model resolution: 12.5 km
  - Data assimilation system: 4dvar
  - 10 days forecast: 00, 12 UTC
  - Five days forecast: 06, 18 UTC
- **CMA-GFS Data Assimilation System**
  - 4DVAR
  - Observation Operators:
    - ARMS 1.2
    - RTTOV 13.2
- **Conventional vs Satellite Data**
  - Raobs, Buoy, aircraft, ground-based MW, ground station data
  - NOAA/METOP/FY-3 IR/MW Sounders
  - GOES/METEOSAT/AHI/FY-4 data
  - GNSS, GNSS-R, METOP/FY/HY Scatterometer
  - Commercial satellite data
  - …

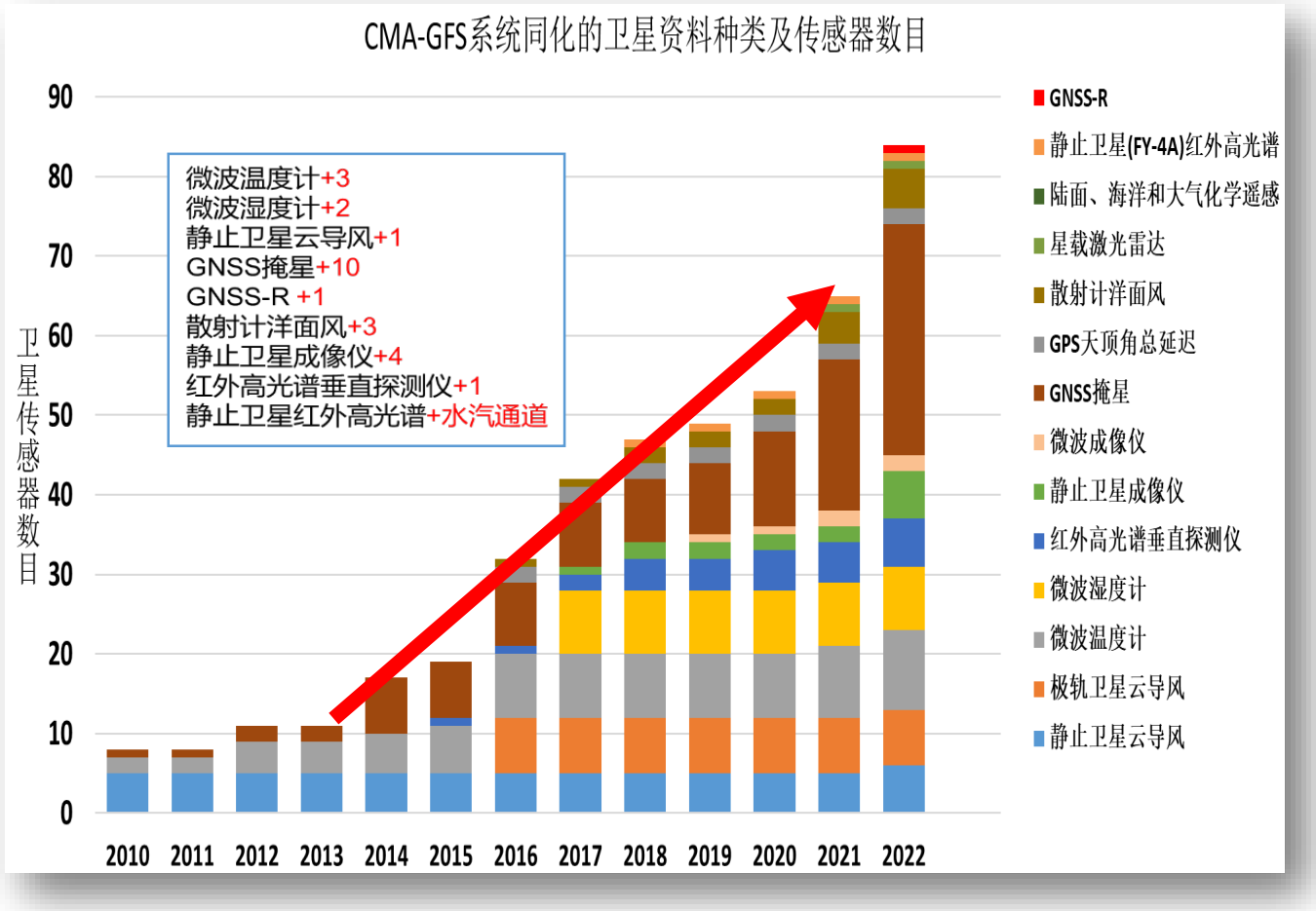

Important Aspects when a New Observation Operator Implemented in CMA GFS

- Some QC thresholds affected by the observation operator should be revised carefully for each instrument
- Cloud screening related to the observation operator should be properly adjusted according to each instrument
- Bias correction schemes require further refinements since each observation operator has its own simulation accuracy
- More importantly, the data entering to the NWP systems should remain comparable when a new operator is implemented.

AMSU-A Performance in CMA GFS Using ARMS

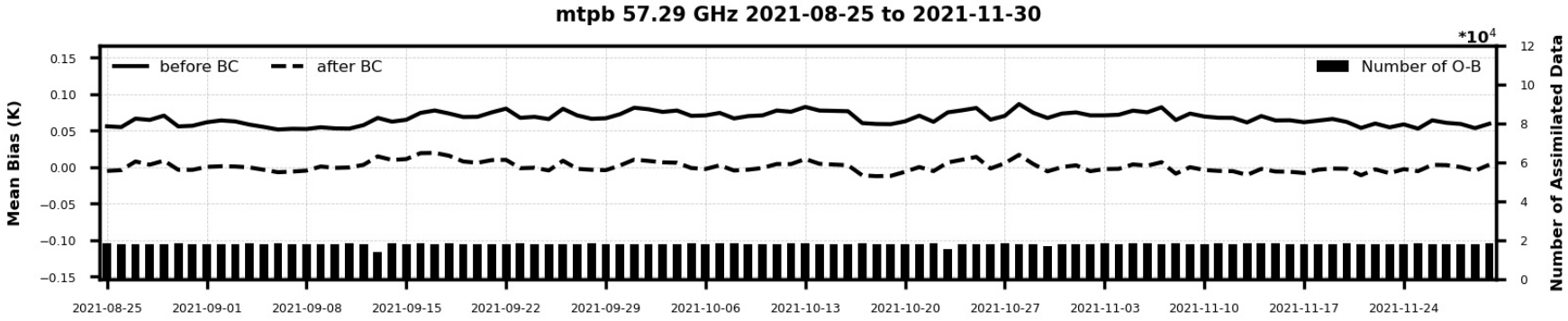

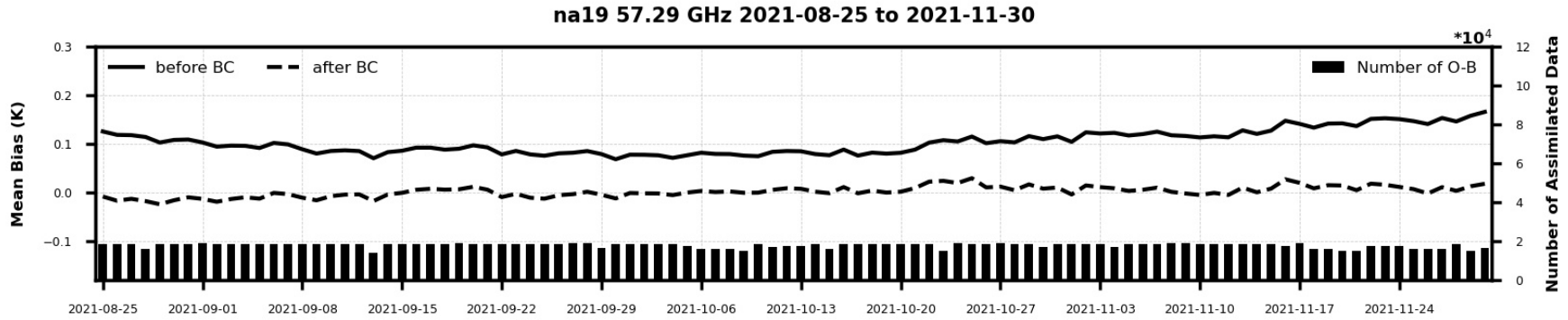

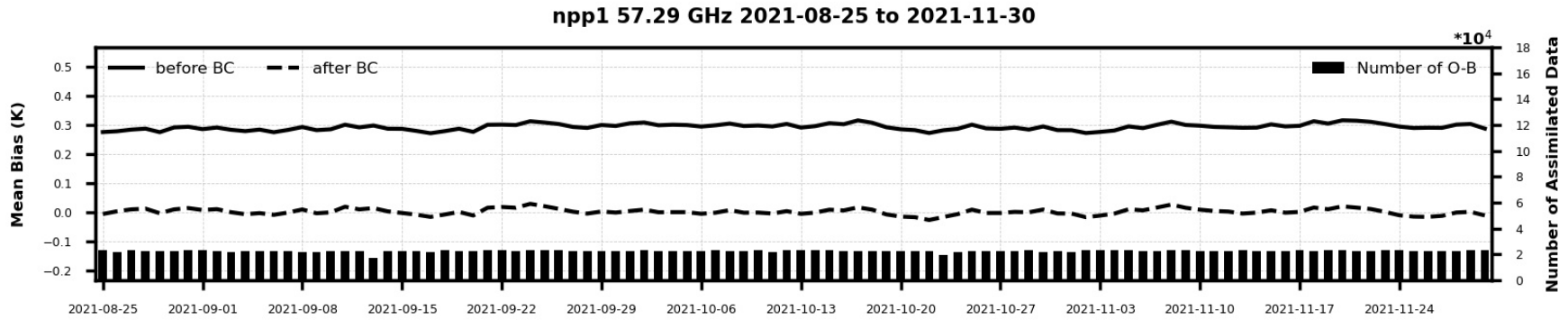

NOAA-20 CrIS Performance in CMA GFS Using ARMS

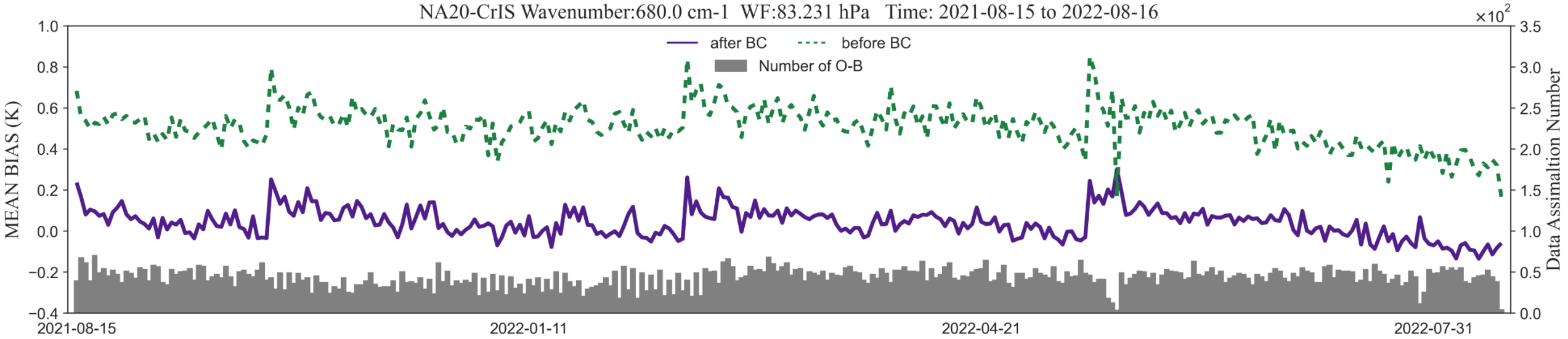

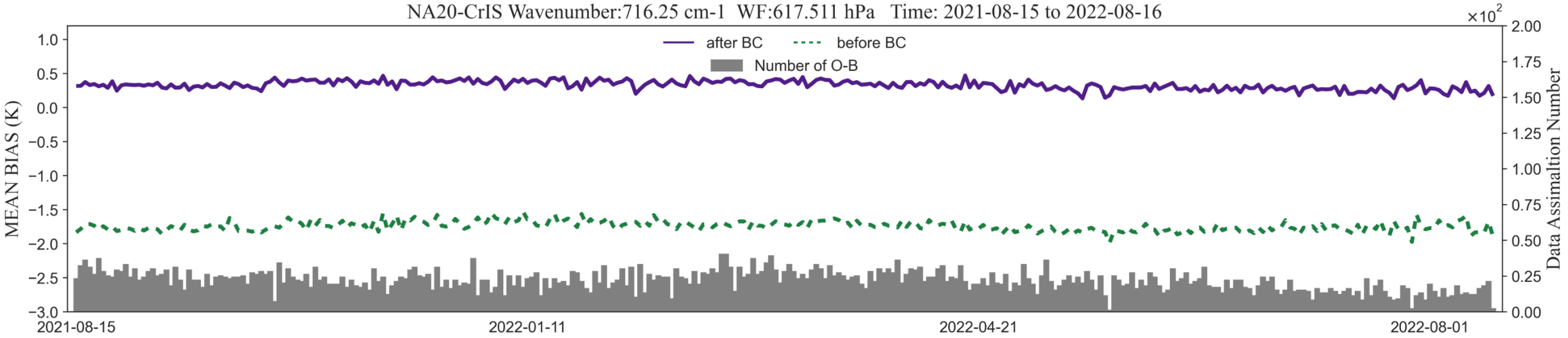

MetOP-C IASI Performance in CMA GFS Using ARMS

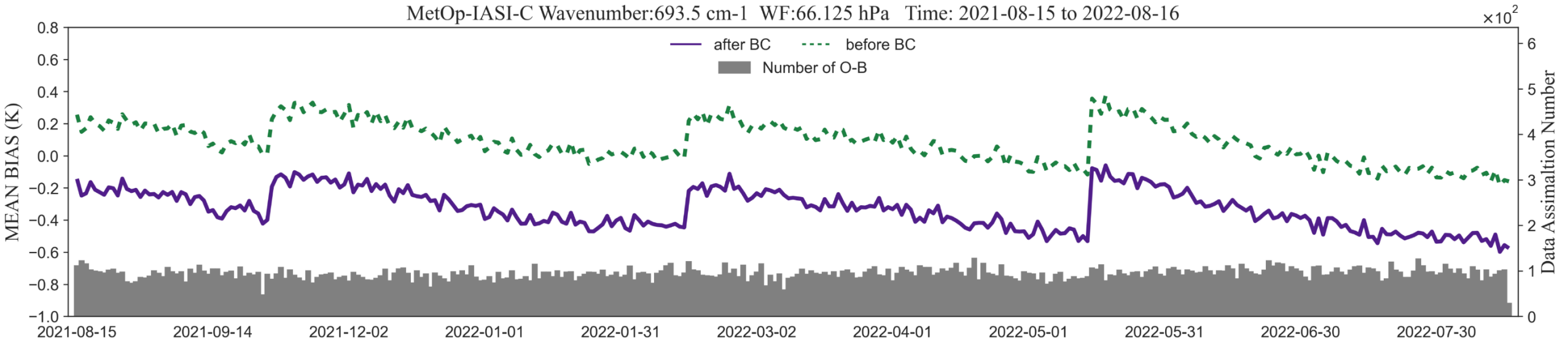

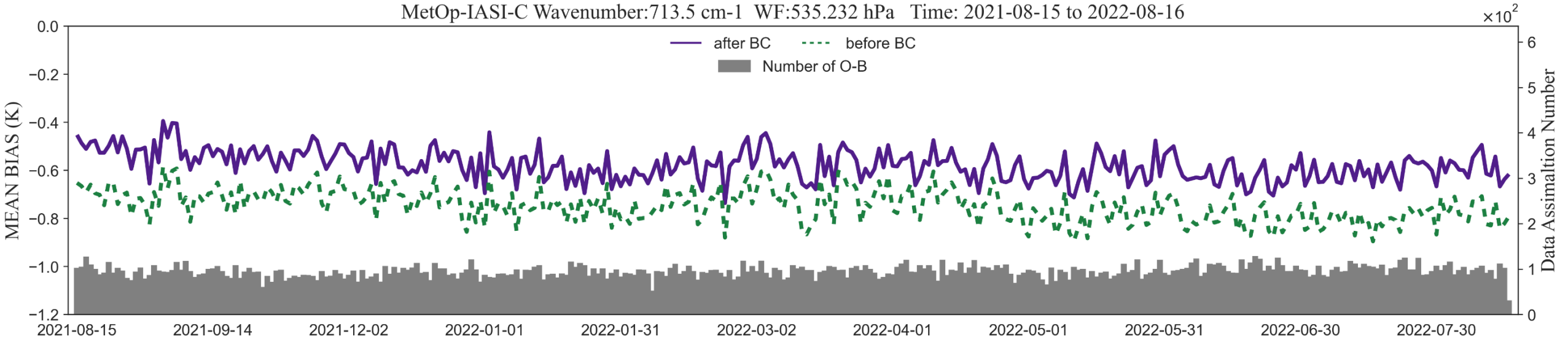

FY-3D HIRAS Performance in CMA GFS Using ARMS

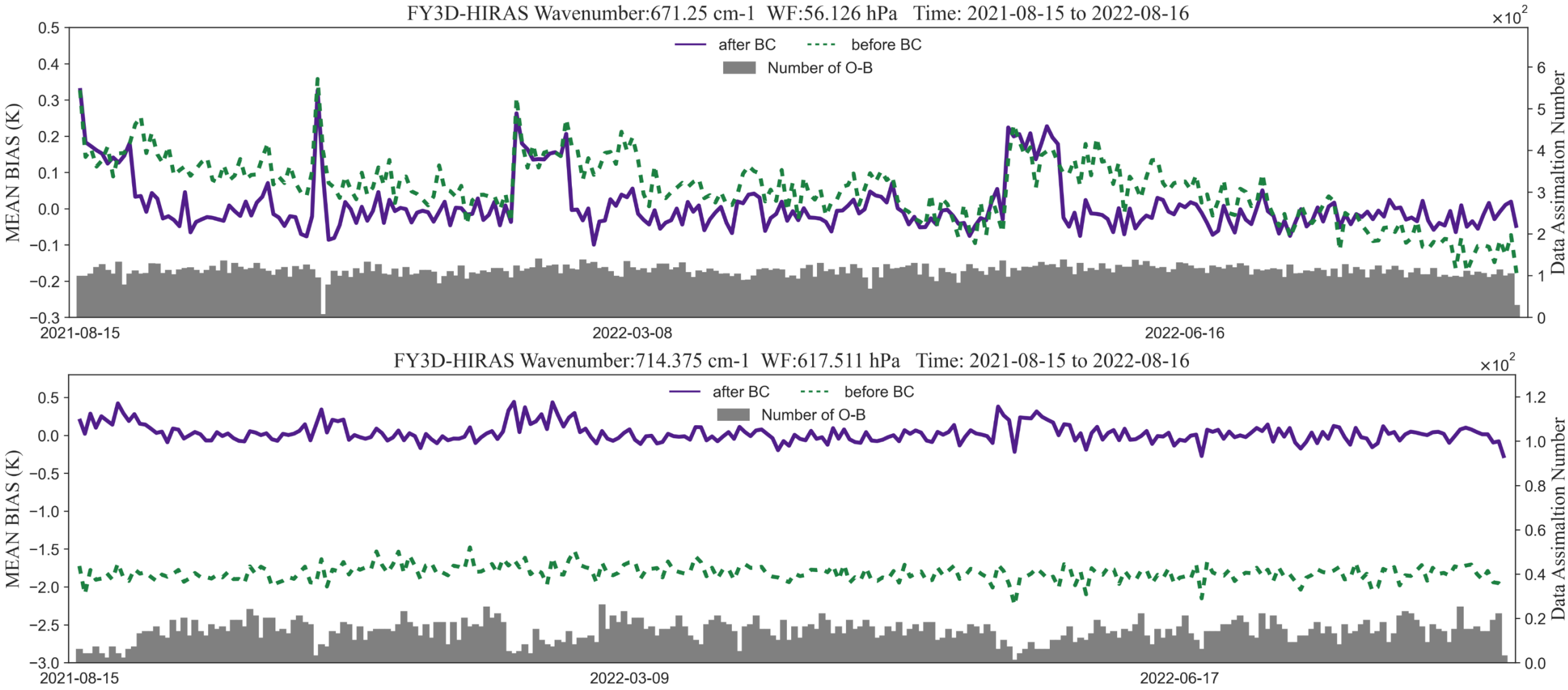

FY-3E MWTS-II, MWTS-III vs. Suomi NPP ATMS O-B

Based on simulation results within 25S-25N region from 2022-03-15 to 2022-04-15.

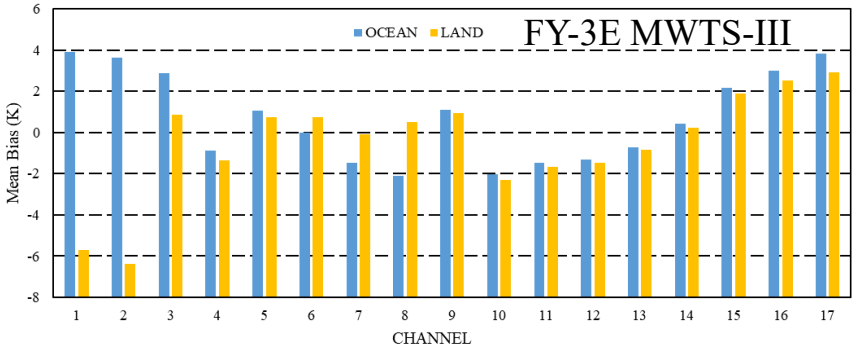

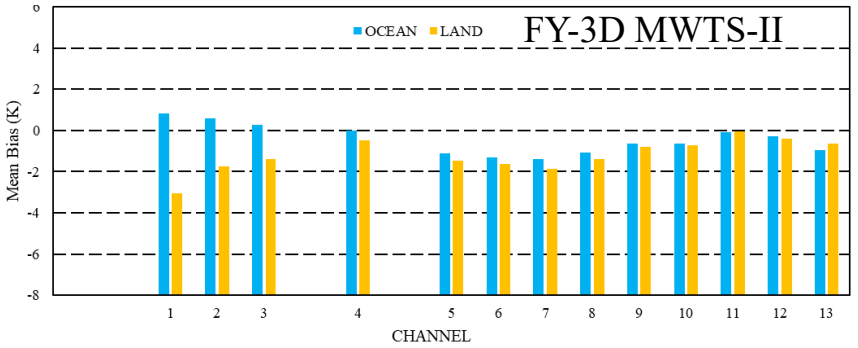

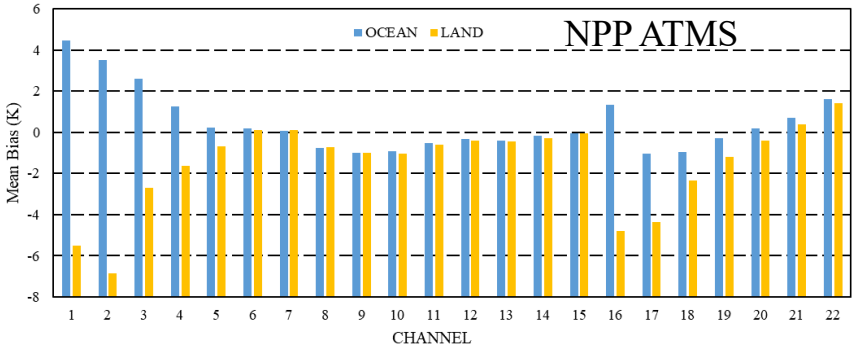

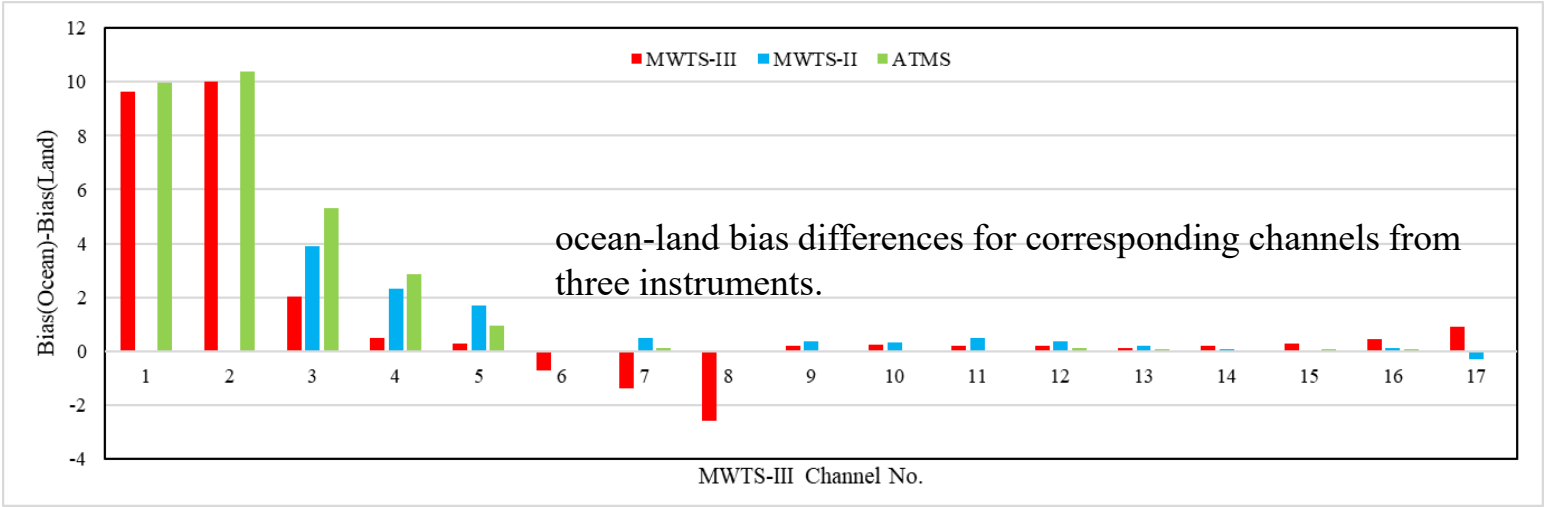

For sounding channels, the ocean-land differences are obvious for MWTS-III channels 6 to 8, especially for channel 8 which has a difference larger than 2.6 K.

The ocean-land differences of the common MWTS-II (Channel 5) and ATMS (Channel 6) frequency are 0.5 K and 0.1 K, respectively.

Assessment of FY-3E MWTS-III

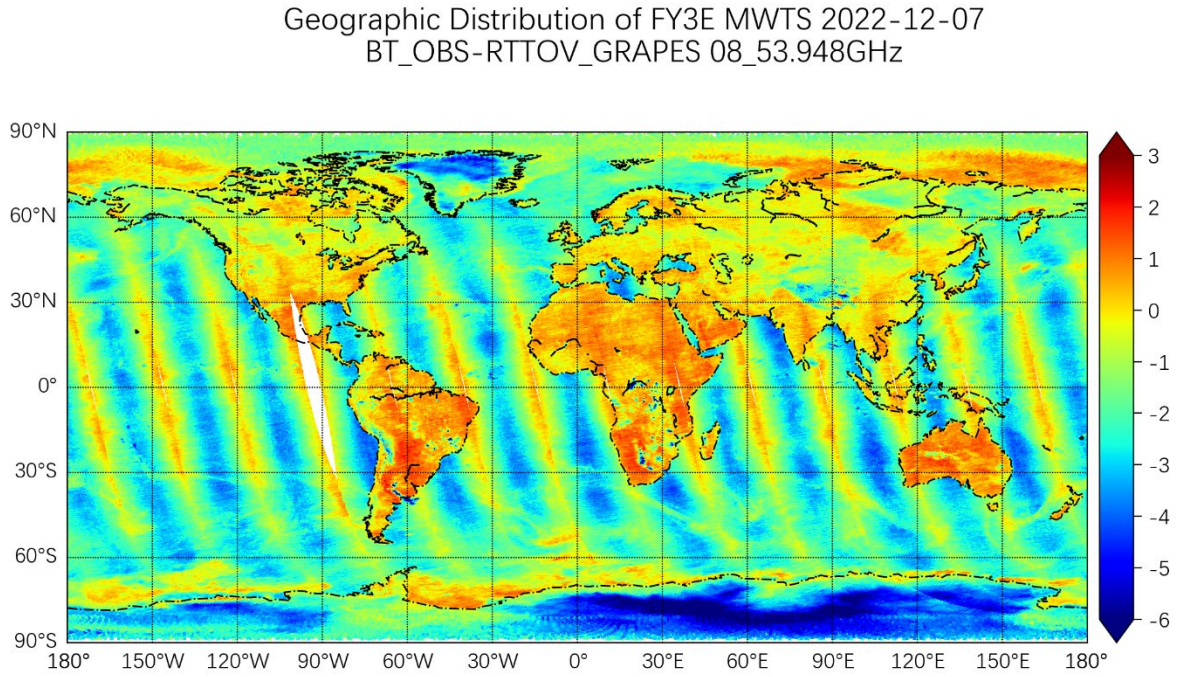

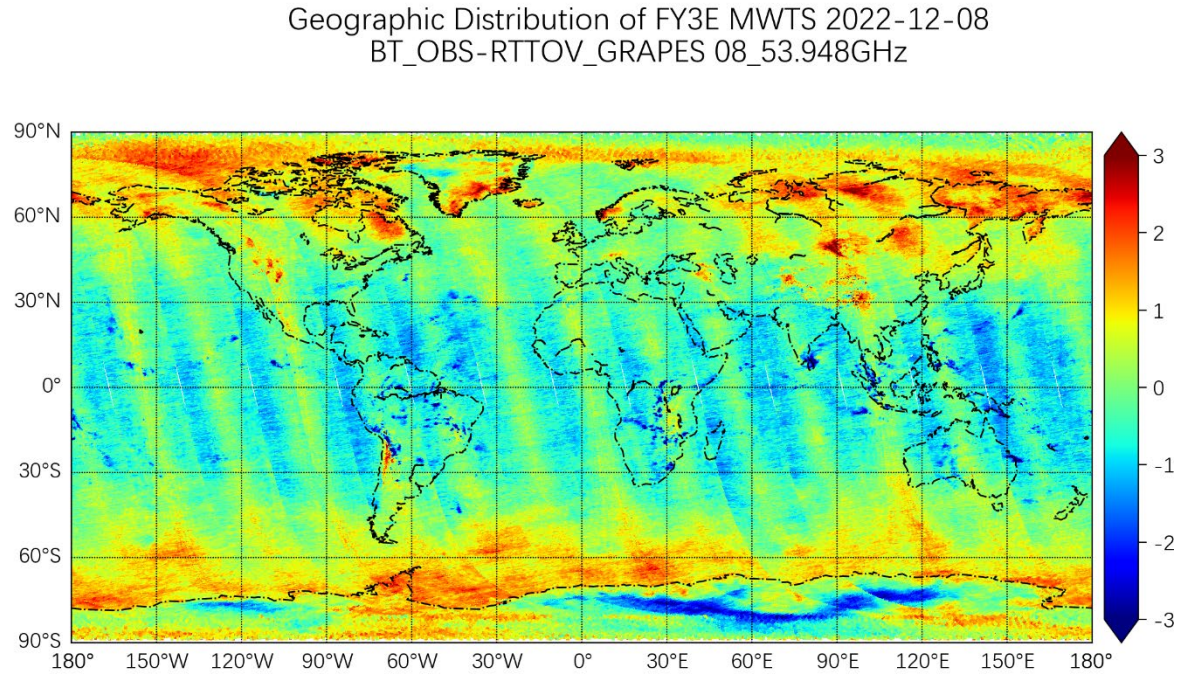

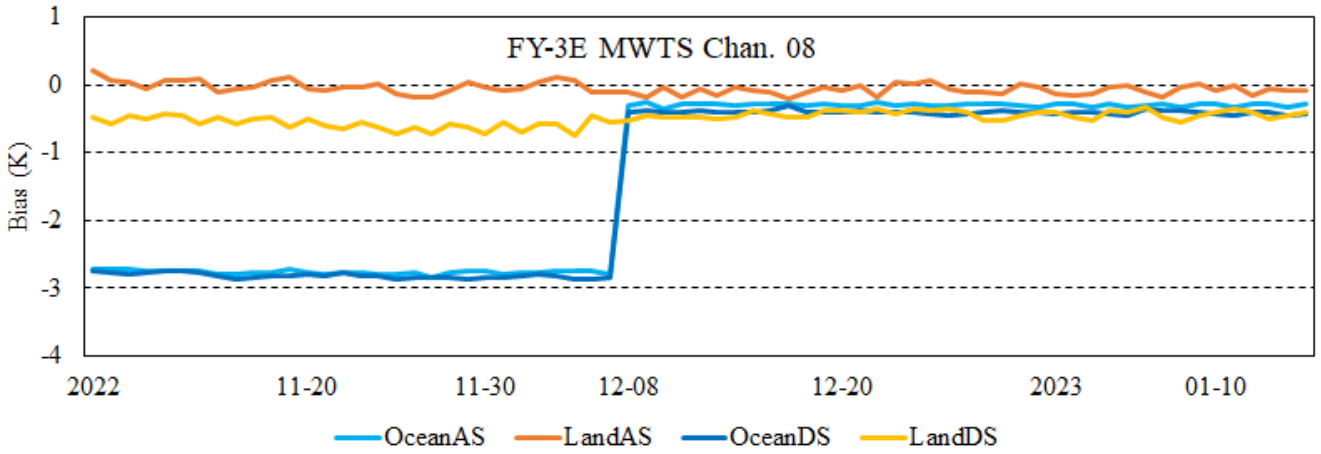

After updating the L1 dataset, the FY-3E MWTS ocean-land issue **has been fixed since 2022-12-08.**

Taking Chan. 08 as an example, the ocean-land bias difference was reduced from 2.5+ K to **less than 0.3 K** since 2022-12-08.

Assessment of FY-3E MWTS-III Radiances against Those Simulated from COSMIC Atmospheric Profiles

- **Time period :**

  2022. 06.01 - 08.31

- **Collocation with COSMIC :**

  Time difference < 3 hour

  Spatial distance < 50 km

- **Clear sky condition:**

  CLW<0.05 (for MWTS)

  SI < 5 (for MWHS)

- **Spatial range:**

  60S-60N over the ocean

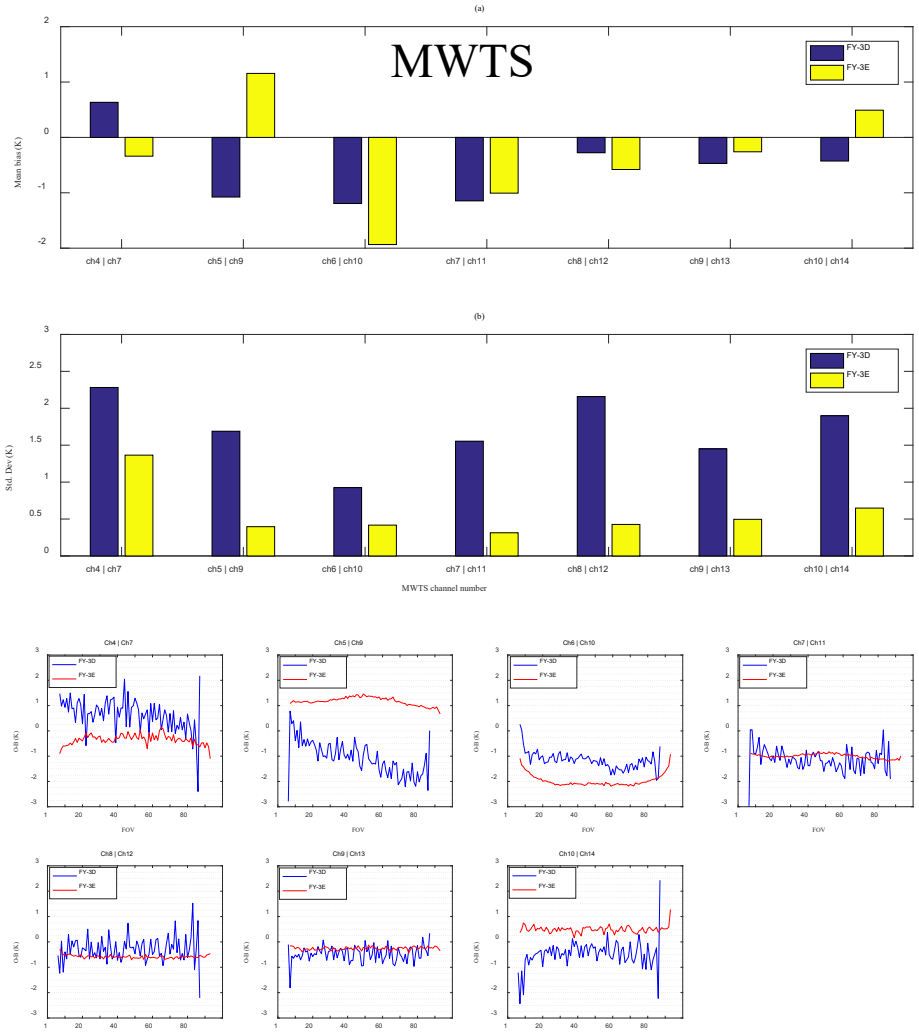

The noises of temperature and humidity channels of MW sounders onboard FY-3E are significantly reduced compared with FY-3D.

The asymmetric bias distribution in the cross-track direction is also significantly improved for FY-3E MW sounders.

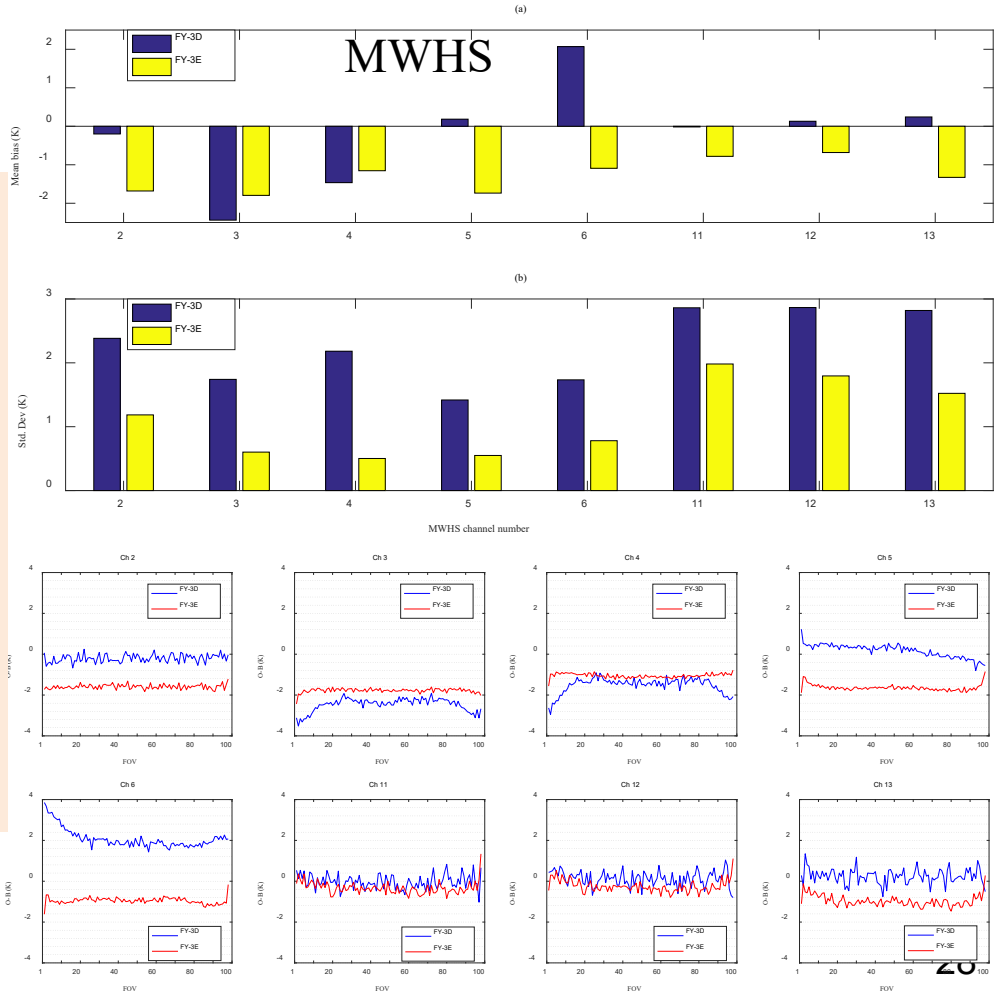

Impacts from FY-3E MWTS-III Data on CMA Forecast

- Unique orbit in early morning
- Data quality much better than FY-3D
- Uses of new MWTS-III Ch 1 and 2 for quality control

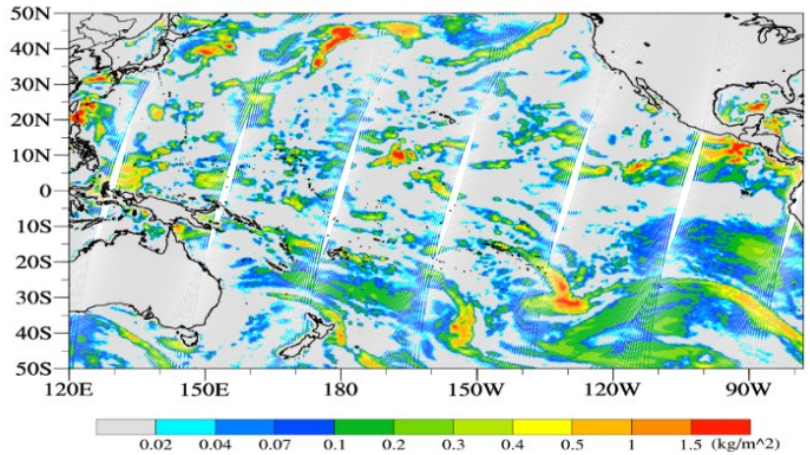

Cloud liquid water from MWTS Ch1 and ch2

FY-3E MWTS/MWHS on Height Analysis

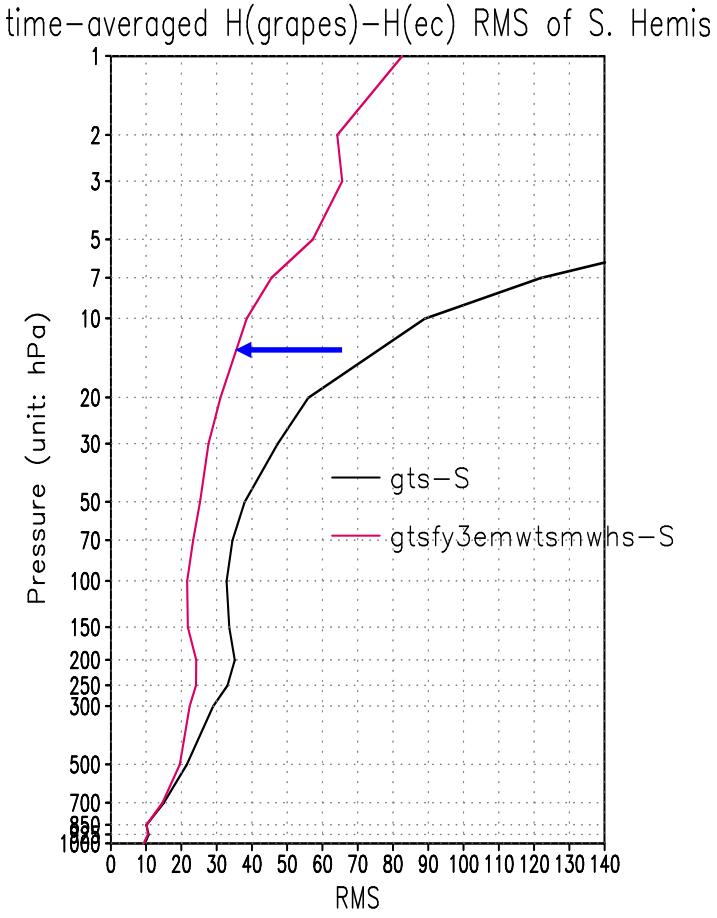

Score card from FY-3E MWTS/MWHS

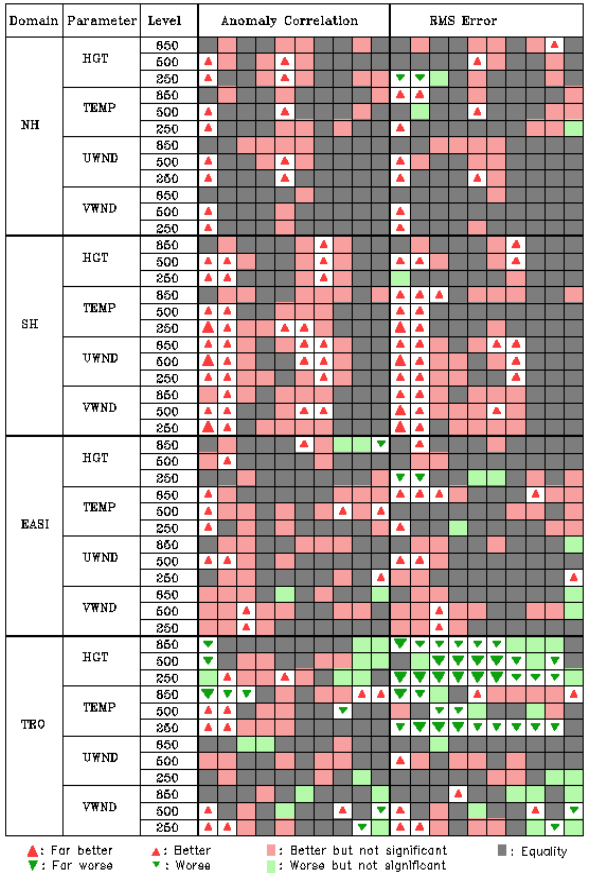

See Dong and Weng, 2022; Remote Sensing

Impacts of ARMS in CMA-GFS 4DVAR on ACC at 500 hPa

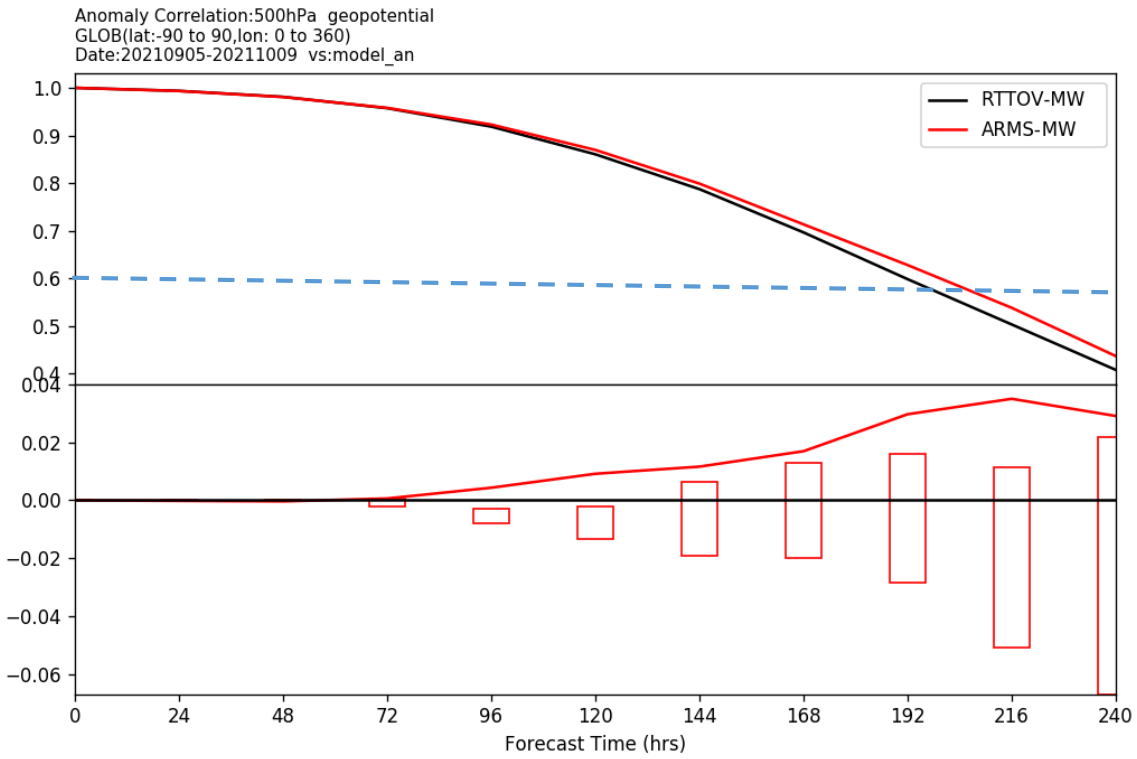

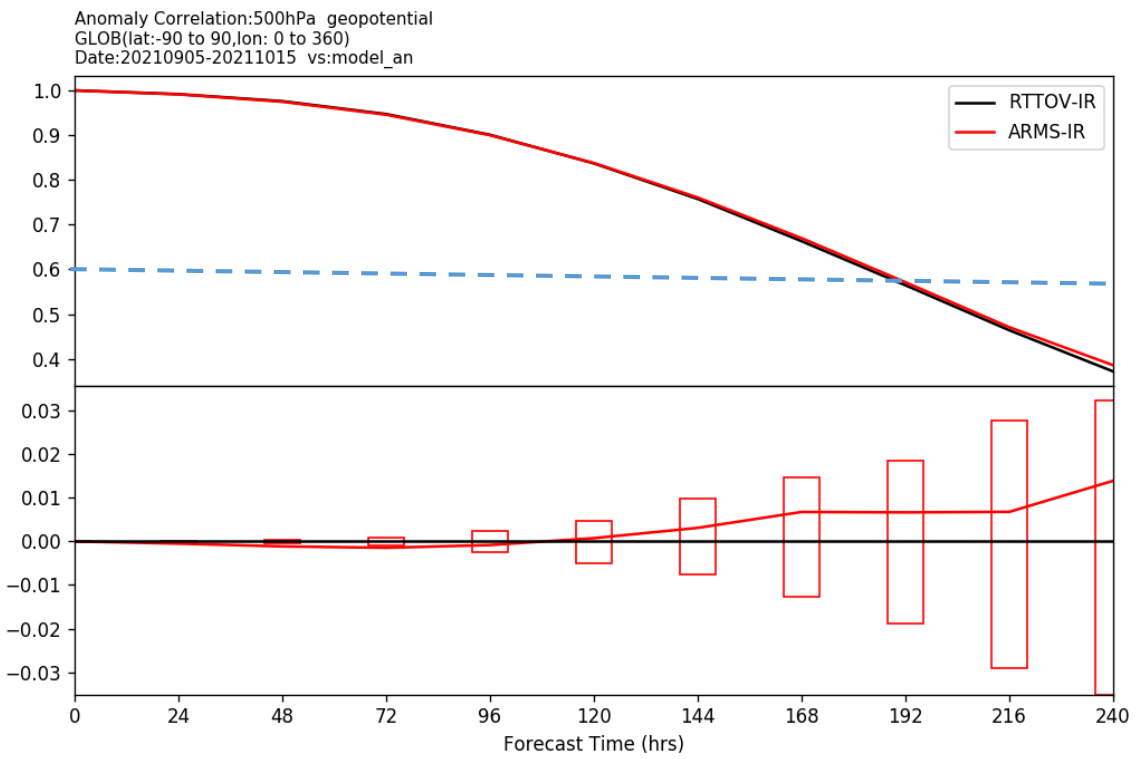

- 45 days of experiments from 9-1 to 10-15 in 2021.
- For assimilation of microwave sounding data, uses of ARMS can extend the forecasting period by about 4-6 hours in CMA-GFS.
- For assimilation of infrared data, the forecasting scores from ARMS and RTTOV are similar

Summary and Conclusions

- ARMS is integrating the state-of-the art radiative transfer sciences into its software design and includes many plug-and-play modules, allowing for community to contribute its future developments;

- ARMS ocean polarimetric pBRDF model can calculate ocean emissivity, normalized radar cross-section for both active and passive microwave data assimilation and remote sensing applications;

- ARMS has been fully integrated into CMA GFS 4dvar system and is now supporting the assimilation of both infrared and microwave instruments;

- Impacts of ARMS on assimilation of microwave data in CMA GFS are very positive and will become part of CMA GFS 4DVAR to support more increasing volumes of data from Fengyun, Haiyang and many international commercial satellites